



Research Article

## Accelerated solidification of PCM via Al<sub>2</sub>O<sub>3</sub>/CuO hybrid nanoparticles in triplex tube heat storage

Ibrahim E. SADIQ<sup>1</sup>, Sattar ALJABAIR<sup>1,\*</sup>, Abdulhassan A. KARAMALLAH<sup>2</sup>

<sup>1</sup>Department of Mechanical Engineering, University of Technology, Baghdad, 10066, Iraq

<sup>2</sup>Department of Mechanical Engineering, University of Al Salam, Baghdad, 10010, Iraq

### ARTICLE INFO

#### Article history

Received: 27 May 2023

Revised: 19 August 2023

Accepted: 30 August 2023

#### Keywords:

Hybrid Nanofluid; PCM; Phase Change Material; Solidification; Triplex Tube Heat Storage

### ABSTRACT

The thermal performance and heat transfer augmentation of paraffin wax as a phase change material (PCM) throughout discharging process within a triplex tube heat storage have been examined using a combined experimental and numerical analysis. The efforts of this research are focused on using a blend of two different types of highly conductive nanoparticles (Al<sub>2</sub>O<sub>3</sub>/CuO hybrid nano additives) to enhance the thermal characteristics of paraffin and improve the overall performance of TTHS, which is the originality of this study. Various volume concentrations (0.4, 0.8, 1.6, 3.2%) of hybrid nanoparticles were explored. Besides that, A set of tests were carried out to evaluate the impact of changing inlet temperature and mass flow rate of the heat transfer fluid (HTF) on the phase change phenomenon of the paraffin. The mass flow rates of HTF ranges from 3 kg/min to 12 kg/min while the temperatures of HTF varies from 30 °C to 40 °C. The calculations are included an iterative, finite-volume numerical technique that involves a domain enthalpy porosity model to simulate the phase transition process. The agreement between the experimental data and the numerical simulation is good. According to the results, reducing inlet temperature and/or increase the inlet mass flow rate of HTF speed up solidification rate. However, HTF inlet temperature has more impact on solidification rate than inlet mass flow rate. Moreover, the reduction in freezing duration caused by implementing hybrid nanoparticles has been observed for all volume concentrations investigated. However, adding 3.2% volume percentage of hybrid nanoparticles results in the highest overall freezing time reduction (about 23%).

**Cite this article as:** Sadiq IE, Aljabair S, Karamallah AA. Accelerated solidification of PCM via Al<sub>2</sub>O<sub>3</sub>/CuO hybrid nanoparticles in triplex tube heat storage. J Ther Eng 2024;10(4):880–903.

### INTRODUCTION

Nowadays, fossil fuel plays a major role in energy production of the world. However, this energy is limited in quantity and produces high level of pollution. Therefore,

developing a suitable source of energy is crucial to overcome these issues. The two most efficient sustainable and renewable sources of energy are solar and wind systems, which have very beneficial applications, for instance, air conditioning systems in buildings and solar water

#### \*Corresponding author.

\*E-mail address: [Sattar.J.Aljabair@uotechnology.edu.iq](mailto:Sattar.J.Aljabair@uotechnology.edu.iq)

This paper was recommended for publication in revised form by Editor-in-Chief Ahmet Selim Dalkılıç



heaters [1]. Since these systems are periodic during the day and the energy demand varies over the day, a temporal inequality between energy supply and energy demand could be created. Therefore, energy storage systems are useful for matching this imbalance and promoting larger utilization of the mentioned sources [2]. In general, there are three main forms of storing thermal energy, sensible heat in which the temperature of storing material changes throughout charging /discharging, latent heat that storing/releasing energy achieved when the storage substance changes its phase from solid to liquid (charging) or from liquid to solid (discharging), thermochemical storage based on the principle of reversible exothermic and endothermic chemical reactions for heat storage [3,4]. Among the aforementioned forms, latent heat storage has been determined to be very attractive in terms of high energy storage ability over a narrow temperature difference [5,6], almost isothermal phase transition process [7], and running in a many cycles with no significant changes in its thermal and chemical properties [8]. In fact, for a given volume, PCMs are able to store 5–14 times more thermal energy than sensible heat substances [9]. This feature is beneficial, specifically for applications that require a small space. Currently, PCMs have drawn a lot of attention due to their uses in a variety of applications, including storing of solar energy [10,11], recovery of waste energy [12], electronic equipment cooling [13], and energy-efficient constructions [14]. However, the poor thermal conductivity of PCM causes slow rate of phase transition, which is a main weakness for their practical uses [15,16]. To solve this issue, several strategies have been adopted to augment the heat transfer in PCMs, such as utilizing fins [17,18], heat pipes [19,20], highly conductive metal foam [21,22], nanoparticles [23,24], graphite composites [25,26], and carbon nanotubes [27,28] as classified in Figure 1. However, it must be realized that adopting these methods need carefulness. They may cause undesirable consequences in term of decreasing the quantity of PCM in storage, increasing the weight of storage, and altering the flow regime.

Moreover, there is another problem regarding PCM usage is that majority of these materials produce considerable density variation during phase change [29]. This problem, in the majority of cases, causes unfavorable expansion and shrinkage of the PCM throughout melting and solidification. Consequently, additional stresses are applied on the surface of storage. The problem is frequently resolved by making an air gap inside the container to permit the storage material to expand freely without exerting extra force against the inner surfaces of the storage [30,31]. However, with several cycle of charging and discharging, a number of air pockets are created in PCM during solidification. These air pockets adversely impact on the characteristic of heat transfer and uniformity of material which must be maintained for long-term operation [32–34]. The main focus of the current work is to comprehend the impact of utilizing

nanoparticles as additives to improve PCM solidification. As a result, the effect of air pocket creation throughout the solidification phase was not taken into consideration in this numerical study. However, it was impossible to avoid it in experimental study.

The use of an extended surface to improve heat transfer is superior due to ease of implementation and comparatively low production cost. Annular, longitudinal, pin, and plate are the most popular fin designs. Among them, the longitudinal fins are performed well, particularly for cylinder shape storage [35]. The impact of perforated fins on the efficiency of vertically oriented shell and tube heat storage was investigated by Karami and Kamkari [36]. According to the experiment, PCM in the storage with perforated fins melted completely in 7% shorter duration than the storage with plain fins. This was ascribed to free convection movement in the holes of fins. Khan and Khan [37] investigated the thermal characteristic of the shell and tube storage coupled with various orientations of the Y-fins configuration using both experimental and numerical methods. The quantitative result showed that 50.7% reduction in charging time and 10% augmentation in the capacity of thermal storage can be obtained as fins arrangements changing from  $\lambda$  to Y. Yousef et al. [38] carried out a study on the acceleration of the melting rate in PCM-based solar still by coupling hollow pin type fins to the unit. Experimental tests were conducted for typical and pin-finned PCM-based units in order to assess the rate of heat transfer. In the result, an enhancement of 17% by employing pinned shape fin in comparison to typical unit. Liu et al. [39] suggested an innovative ladder-shaped fin to speed up charging process for waste heat recovery system. The numerical result revealed that ladder-shaped fins are more effective than straight fins at optimizing the charging channel of PCM. Moreover, the highest reduction of total charging duration was 52.2% in comparison to the straight fin. A novel tree-pin-shaped fin in a shell-and-tube storage system was designed and built by Wu et al. [40]. Adipic acid as PCM was implemented in the shell. For comparison purposes, traditional longitudinal fins were also investigated under the identical conditions. It was found that tree-pin-shaped fins promote melting and solidification rates and make the PCM temperature more uniform. Furthermore, storage with tree-pin-shaped fins reduces the melting duration by 44.6% and the solidification duration by 50.0% in comparison to storage with longitudinal fins. Mahdi and Nsofor [41] utilized aluminum foam of 0.95 average porosity to promote charging and discharging rate in shell and tube heat storage. Findings showed that increasing the cascade number has a significant impact on the phase transition process, which shortens the charging and discharging durations. Moreover, existing metal foam reduce the temperature variation across PCM. In general, the existence of extended surfaces or metal foam in PCM may resist the growth of the natural current that is induced in the molten region, which in turn

would offset (minimize) the positive impact of extended surfaces on thermal performance of storage. Furthermore, integration of solid material (e.g. fins and porous matrix) reduce the amount of PCM and increase the overall storage weight which deteriorate total storage energy and influence mobility of these units.

Another good candidate, is to boost thermal conductance of PCM by incorporate, conductive nano scale powder, which is shown to be suitable and easy to achieve. Nano-particles, can be categorized, into two, groups: (a) carbon, allotropes and (b) metal-oxides, or metals. [42], .carbides and .nitrides [43]. Hosseinizadeh et al. [44] investigated the melting rate inside a spherical storage employing Cu-RT27 nano-PCM. It was indicated that melting duration dropped by 5 min as volume fraction boost from 0 to 0.04. Dispersion CuO nanoparticles at two volume fractions of 0.034% and 0.5% to speed up the melting of three different organic PCMs, namely, paraffin wax, coconut oil, and RT18 was performed by Al-Jethelah et al. [45]. They determined the four regimes during the melting of nano PCM using a scale-up methodology. Ebadi et al. [46] used coconut oil as PCM inside a cylindrical energy storage to explore the impact of nanoparticle volume fraction and Rayleigh number on the charging phase. It was stated that the total storing energy minimized as nanoparticle increase. Multi-walled carbon nanotubes were added to paraffin by Murugan et al. [47], who exhibited that the paraffin's thermophysical properties were significantly improved by inclusion low concentration of the nanotubes. Another article noted that inclusion 1.0% by weight of carbon nanotubes to the paraffin augment its thermal conductivity by 113.3% [48]. As result, a significant reduction of the total melting and freezing durations was obtained. Gorzin et al. [49] examined the freezing of Cu-RT50 nano-PCM in multi-tubes thermal storage with different configurations of paraffin in the tubes. The freezing time shortened about 15% by incorporating nanoparticle of 0.04 volume concentration. Hamza and Aljabair [50] indicated that the addition of two various kinds of nanoparticles has a strong tendency to boost heat transmission owing to their synergistic effect. The melting and freezing of the  $Al_2O_3$ , AlN, and GNP-paraffin nano-PCMs in shell and tube heat storage were conducted by Khan and Khan [51]. In comparison to PCM without nano, melting time reduction of about 28.01%, 36.47%, and 44.57% for  $Al_2O_3$ -PCM, AlN-PCM and GNP-PCM, respectively. Moreover, the freezing time decrease by 14.63%, 34.95%, and 41.46%, respectively. The same thermal storage system but in another research, Khan et al. [43] tested the influence of inclusion different metal oxide nano powder with volume fraction of 0.01, 0.03, and 0.05 on melting and freezing rates of PCM. Their result indicated that in spite of raising the concentration of nanoparticles augmenting the melting and freezing rates, the free convection diminished. When compared to the pure PCM at concentration of 0.05, The  $SiO_2$ -PCM

had the lowest average melting and freezing durations of all the nano-PCMs by about 41% and 30%, respectively. Hamali and Almusawa [52] applied the Galerkin method to simulate freezing process of fin-assisted water in existence of nanoparticles numerically. Fins of Y-shaped and copper oxide nanoparticles were utilized. Their finding revealed that around 10 % improvement in freezing process was achieved by dispersing these nanoparticles. Likewise, Rothan [53] investigated the effect of shape factor of the CuO nanoparticles on PCM. They found that total freezing time can be decrease by increase shape factor. Quantitatively, about 10% of improvement was obtained by inclusion CuO nanoparticles with the optimum shape factor. Zhao et al. [54] added nanoparticles (CuO) with various electrical charges into paraffin (octadecane) to studied the effect of charged nanoparticles on thermal characteristics of PCM by help of molecular dynamics technique. It was exhibited that thermal conductivity of nano-PCM was significantly enhanced by intensifying nanoparticle charges. Besides that, increasing charge of nanoparticles can enlarge nanolayer thickness. Three different type of nano additives ( $Al_2O_3$ ,  $TiO_2$ , and CuO) and three groups of nanoparticles (mono Nano-PCM, hybrid Nano-PCM, and ternary Nano-PCM) were utilized by Wu et al. [55]. They studied the influence of nanoparticle compound and nanoparticle concentration on the heat transfer and thermal storage performance of shell-and-tube energy storage. The obtained result indicated that charging rate of PCM include multi types of nanoparticles is higher than mono Nano-PCM, by 2.3% for hybrid Nano-PCM and 5.2% for ternary Nano-PCM, respectively.

In the current research, the potential of  $Al_2O_3$  and CuO hybrid nano particle in paraffin is experimentally and numerically performed to evaluate their effect on the freezing process in triplex tube heat storage. Paraffin wax is positioned in the annulus space between the inner and the intermediate tubes whereas cold water is flowing through the inner tube and outer shell. The triplex-tube storage is advantageous over all other type of heat storage in term of high heat transfer area which Intensify heat transfer rate. According to the previous survey, most of the studies focus on using one type of nanoparticles in PCM-based double pipe heat storage. However, the freezing process of hybrid nano-PCM in triplex tube heat storage (TTHS) have not been explored by previous studies. Thus, the novelty of this experiment is to assess the influence of combine two different types of nanoparticles of volume concentration ranged from 0.4% to 3.2% on heat transfer behavior throughout PCM freezing in TTHS. Besides that, the impact of fluid inlet temperature and mass flow rate on the discharging process are also investigated. The major steps of present study are depicted in the Figure 2.

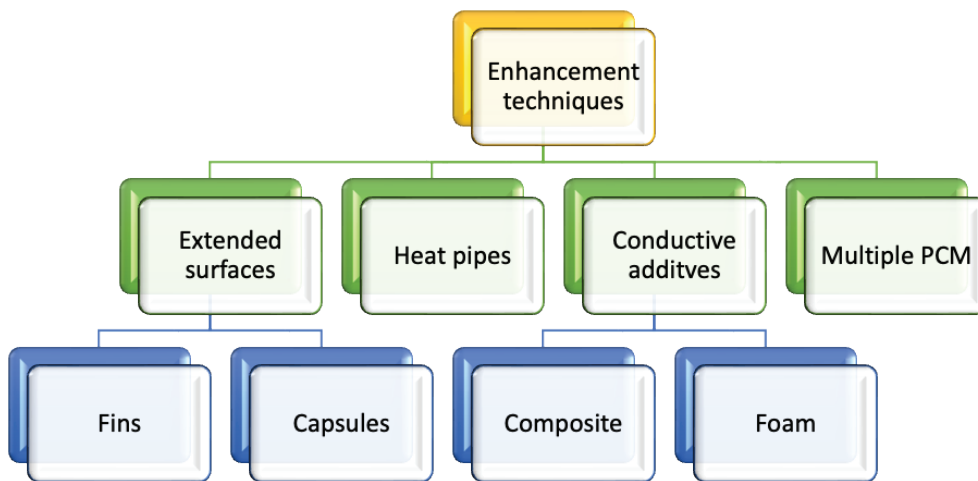


Figure 1. Categorization of augmented methods in PCM based storage units.

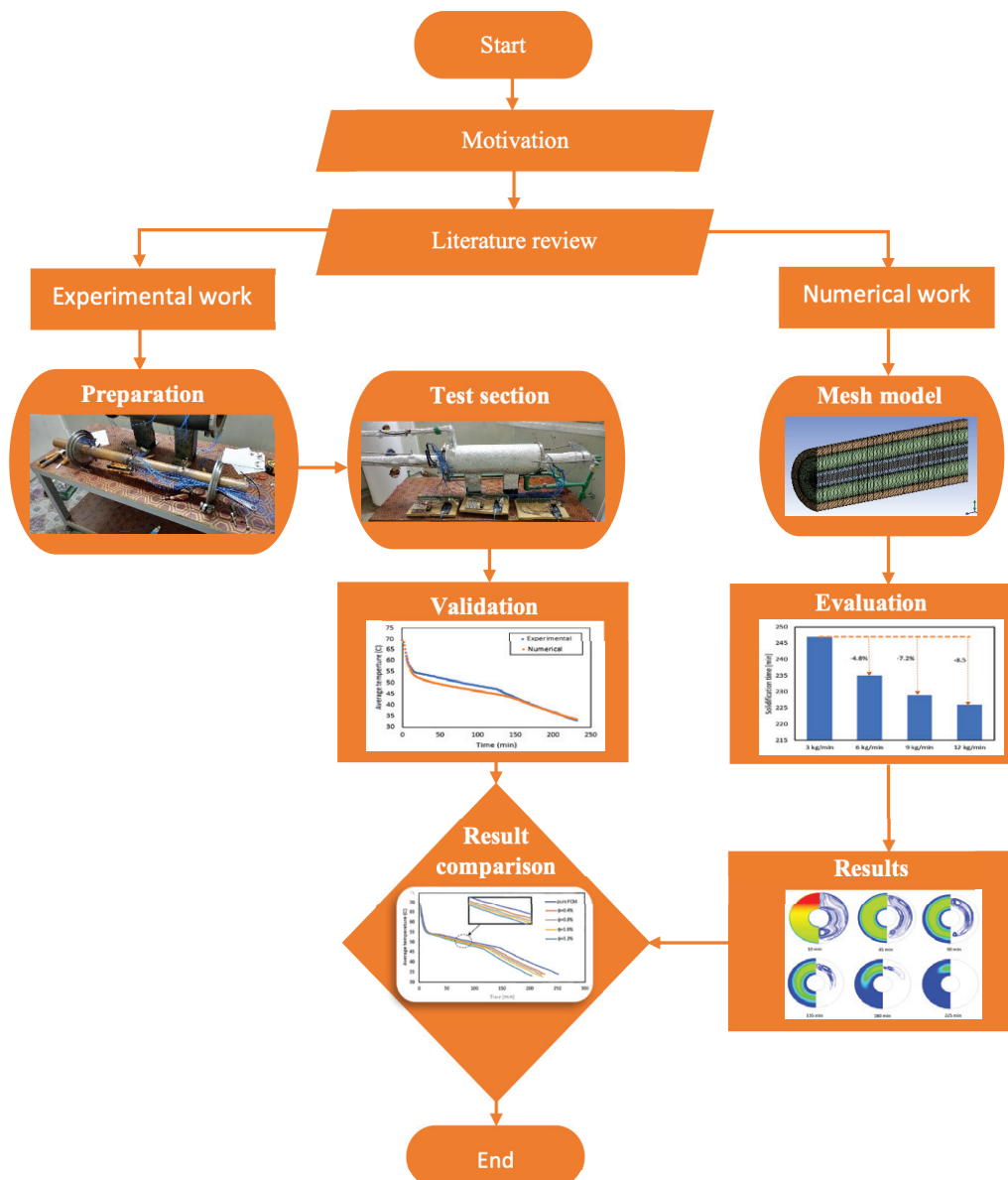


Figure 2. The primary steps of the present work.

## EXPERIMENTAL SETUP AND PROCEDURE

### Experimental Setup

An experimental rig was established to evaluate the thermal performance of triplex tube heat storage. It made up of (1) tank (2) cold water reservoir (3) water pumps (4) flow meters (5) radiator (cross type heat exchanger) (6) thermocouples (7) temperature data recorder (8) triplex tube heat storage, as depicted in Figures 3 and 4. The storage consists of three concentric tubes of 600 mm length oriented horizontally. The PCM of 7 kg occupy annulus space between inner and intermediate tubes while the water flow in the inner tube and outer shell. The diameters of inner, intermediate and outer tubes were 50, 150, and 200 mm, respectively. To achieve high heat exchange between PCM and water, the inner and intermediate tubes were made of copper. However, the outer tube was made of carbon-steel. Two carbon steel flanges were fabricated to seal both ends of storage. Each flange has 53 mm concentric hole to facilitates passing the inner tube.

Glass wool insulation with a 50 mm thickness was covered the storage to reduce the amount of heat dissipation from the storage to the surrounding air. To validate the effectiveness of this insulation, the heat loss should be quantified. This can be achieved by measuring the temperature of outer surface of insulation by using an infrared thermometer. It was found that the highest temperature variation between the outer surface of the insulation and the surrounding air was not exceed 1 °C for all cases. This slight temperature difference implies that the heat dissipation

from storage is negligible and prove the suitability of this insulation for this storage.

Figure 5 depict the locations of thermocouples used to record the temperature of the PCM. Sixty K-type thermocouples were mounted in the PCM at three different sections along the heat storage length. Each section contains twenty thermocouples placed in radial and angular orientation as illustrated in Figure 6. To measure inlet water temperature, a thermocouple prop coupled in the inlet of test section. Besides that, two thermocouples fixed in the outlet of test section to measure outlet water temperature of tube side and shell side. All thermocouples with a temperature recording scope of 0-200 °C were all attached to a data acquisition system, which in turn recorded the temperature every minute and sent the values to computers.

The experimental test apparatus has two kinds of flow meters. Namely, rotameter and turbine flow sensor, see Figure 4B. A rotameter of 0.2 – 18 l/min measurement range was installed vertically after main circulation pump to record the total volumetric flow rate of water. The other type of flow meter is turbine flow sensor model (G1-2) which was mounted in the plastic bypass pipe before the test section to measure the water flow rate on the outer annulus. The sensor can generate electrical pulse whenever water pass through it. Each pulse equivalent to 3.33 milliliters. Therefore, flow rate can be estimated by counting the output pulses from the sensor. This flow sensor that made of chrome can measure flow rate between 1 to 30 l/min and work with temperature range (-25 ~ +80 °C). The flow sensor was linked to the Arduino Uno with programming code

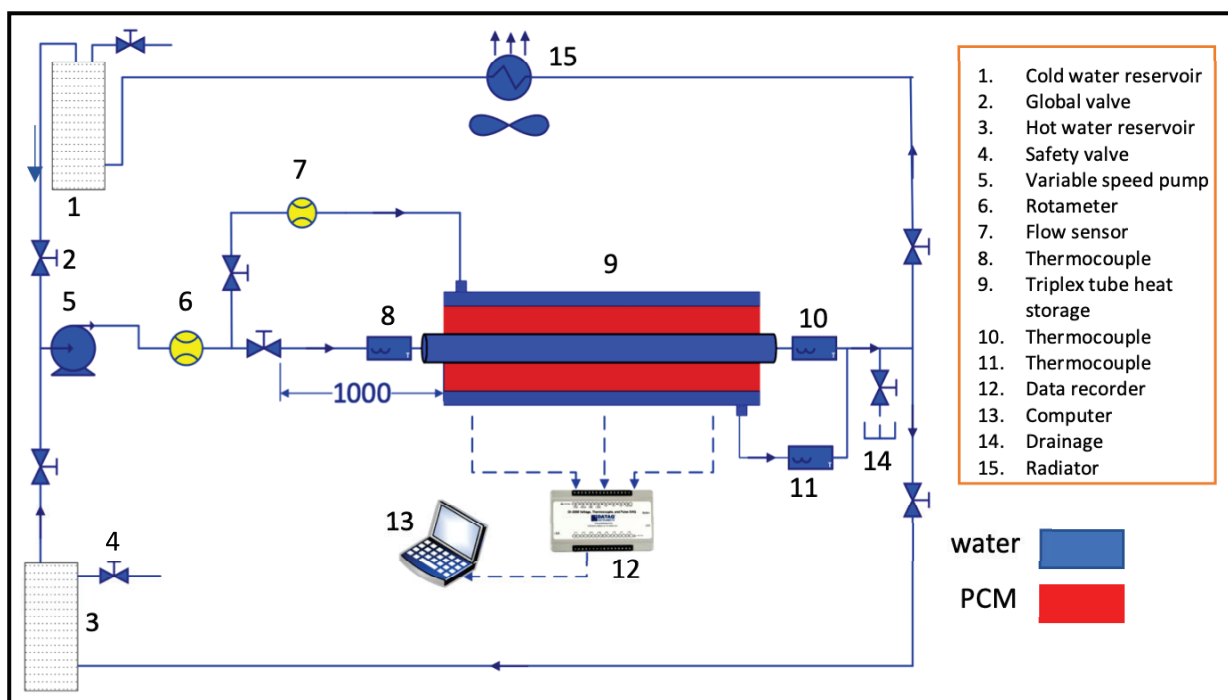


Figure 3. Schematic sketch of test rig.

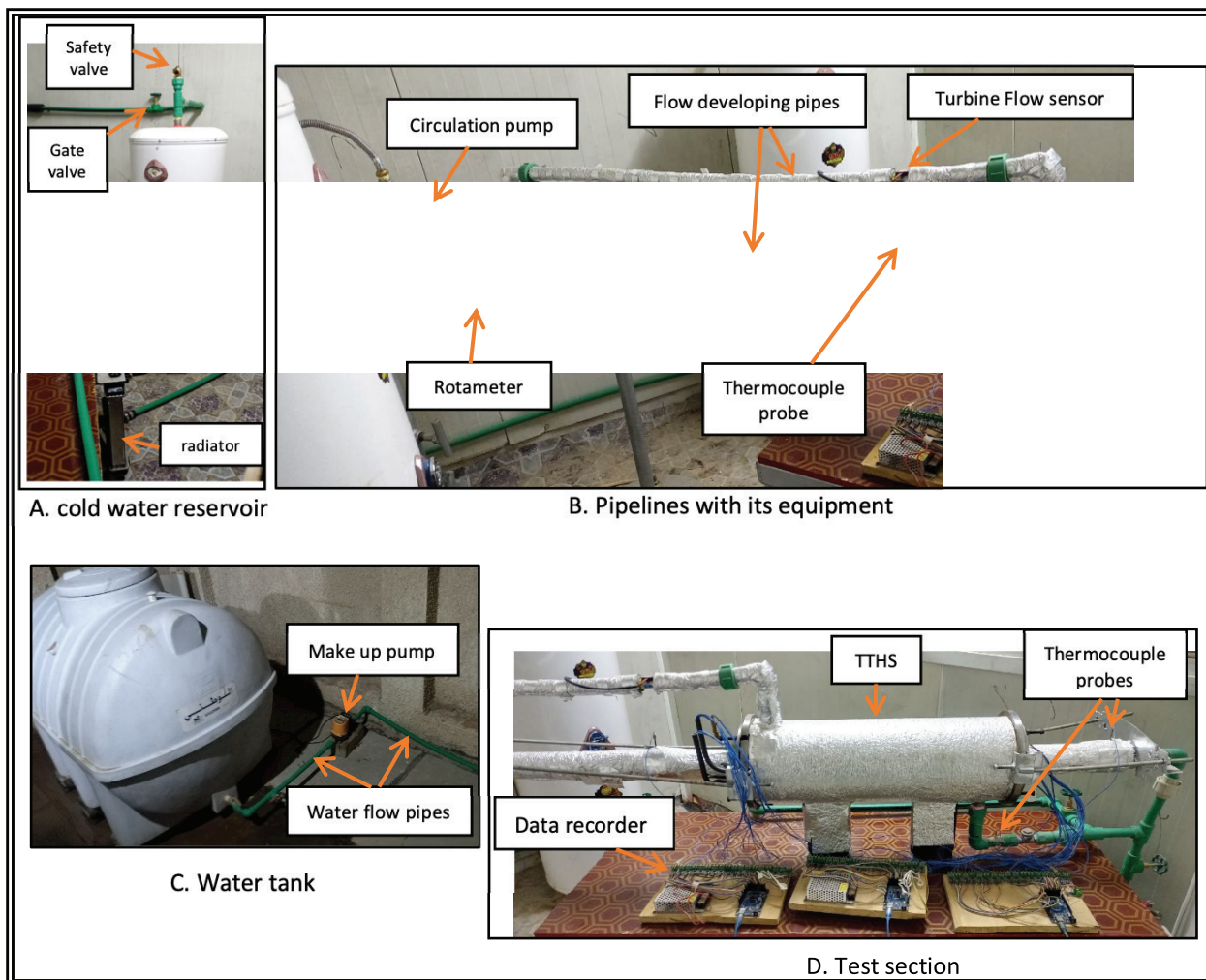


Figure 4. Photo of test rig.

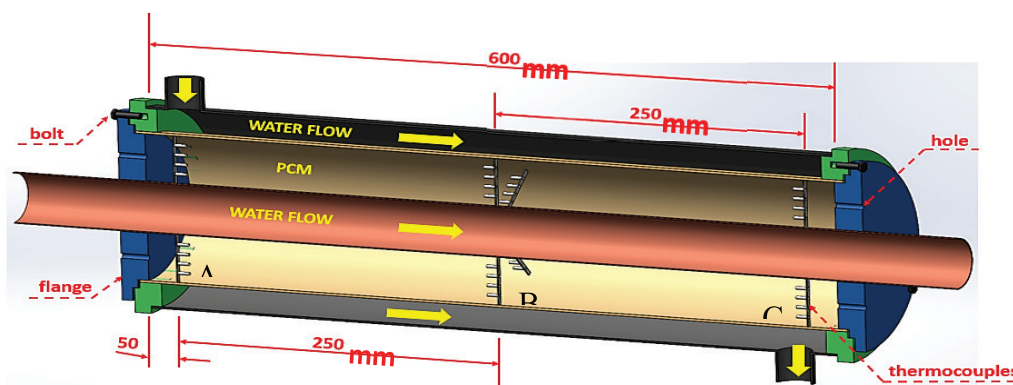


Figure 5. Sectional drawing of TTHS.

saved in it and the result was displayed on the computer. Additionally, Plastic tubes and valves were employed to join the storage to the radiator, cold water reservoir and other components.

**Experimental Procedure**

A 1500 W thermoelectric immersion heater equipped with thermostat installed in the 170-liter water reservoir to control the water temperature during the experiment.

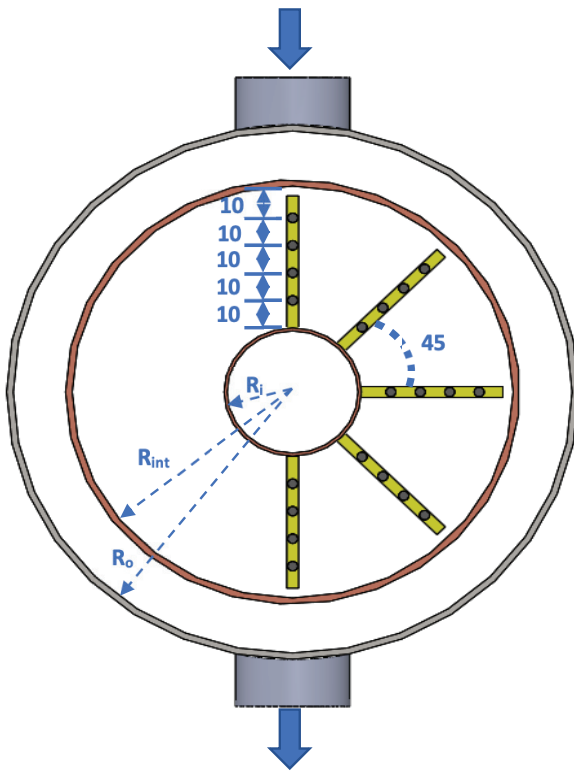


Figure 6. Schematic diagram of thermocouple distribution.

Before start of each test, hot water at 70 °C pumped from the hot water reservoir into the tube and outer annulus of the TTTHS in order to liquify PCM and maintain a constant initial thermal state. This process continued until PCM temperature (thermocouples readings) become higher than melting temperature, which may take around 3 hours. The experiment was commenced by supplying warm water at a predetermined mass flow rate from the constant temperature water reservoir to the TTTHS where water absorb heat from PCM. After that, the heated water flow in radiator to reject the excess heat and keep the cycle temperature constant. The temperature readings of thermocouples were collected by a data acquisition system every 1-minute duration. However, the experiment was stopped when the whole PCM solidified. This can be noticed when all temperature readings of the thermocouples become below solidification temperature and the difference between the outlet and inlet temperature of HTF become less than 0.5 °C. This indicate that PCM reject maximum possible heat and system reach to thermal equilibrium, which may take (4 - 4.5) hours depend on the case. Therefore, the total time required was about 7 hours for complete cycle (charging and discharging).

### Calibration of Measuring Devices

#### Thermocouples

All thermocouples were calibrated by using four substances with defined boiling and melting temperature.

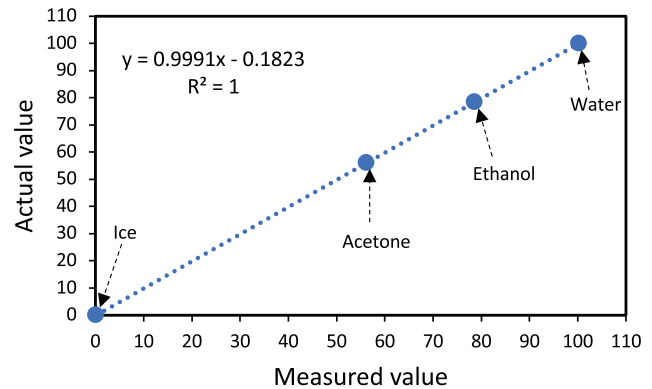


Figure 7. Sample of thermocouple's calibration curve.

These substances were acetone, ethanol, water and ice-water. The instantaneous temperature was measured whenever any of the under-test substances began to boil except ice water which was recorded its temperature during melting. Then, the thermocouple's calibration curve was obtained by comparing the discrepancies between the measured boiling/ melting temperatures and the standard boiling/ melting points. Figure 7 display the sample of calibration curve for one of the thermocouples. The result showed that the average error was  $\pm 0.30$  °C.

#### Flow meters

The calibration of both flow meters was carried out to evaluate the accuracy of both flow meters. This was achieved by utilizing volume scaled vessel and a stopwatch for estimating the time needed to reach a certain volume of water in vessel. The outcomes revealed that the average deviation was  $\pm 0.21$  l/min and  $\pm 0.14$  l/min for rotameter and flow sensor, respectively as depicted in Figure 8.

#### PCM Selection

In the current work, paraffin wax was employed as a PCM provided from China paraffin company. Paraffin is commonly used in literature because it has high latent heat of fusion, non-toxic and chemically stable throughout discharging cycle in comparison to hydrated salts and non-organics paraffin. To determine the specific heat, latent heat of fusion and phase transition range of the PCM, differential scanning calorimetry (DSC) analysis were carried out. The test was performed to a paraffin sample of 14.6 gram in the temperature scope of 40 °C to 900 °C at 20 °C/min heating rate. The DSC thermogram of the paraffin is depicted in Figure 9. By utilizing numerical integration on the area under the curve, the latent heat of fusion is estimated whereas the scope of phase transition can be found between onset point and the point fitting to the peak of the curve. The obtained outcomes from this experiment are given in Table 1.

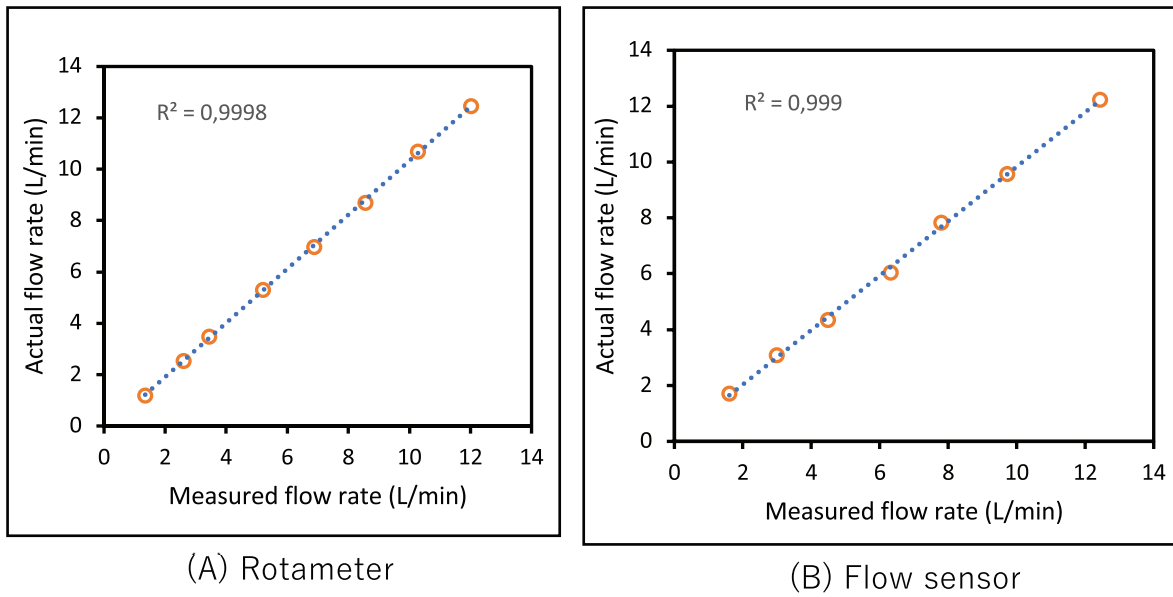


Figure 8. Flow meters calibrations.

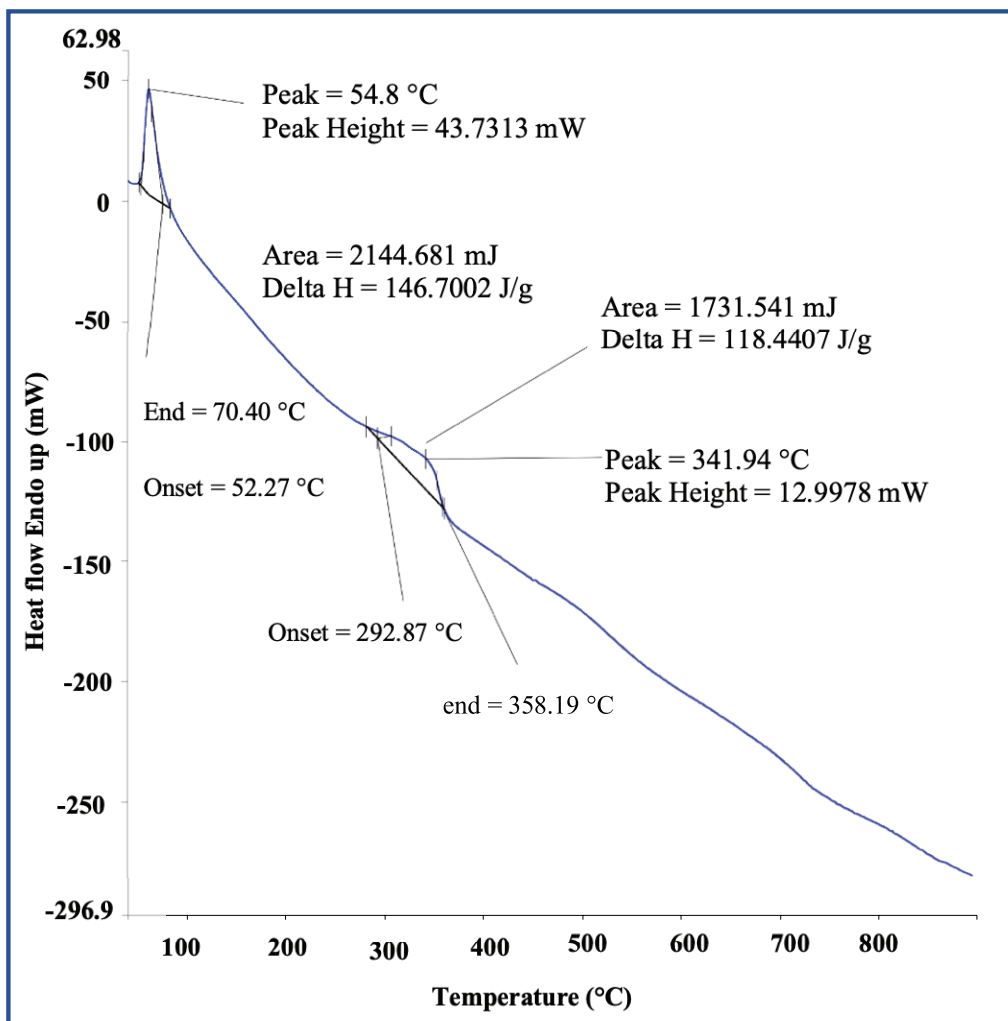


Figure 9. Heat transfer variation vs temperature for tested paraffin wax.

### Preparation of Hybrid Nanoparticles Dispersed Paraffin

$\text{Al}_2\text{O}_3$  and  $\text{CuO}$  nanopowder were purchased from SkySpring Nanomaterials, USA company. Providers were assured that particle size of  $\text{Al}_2\text{O}_3$  and  $\text{CuO}$  of 99.9% purity are 20 nm and 40 nm, respectively. Moreover, the particle shape of two types is spherical. The thermal characteristics of  $\text{Al}_2\text{O}_3$  and  $\text{CuO}$  are given in Table 1.

Figure 10 illustrates the preparation steps of hybrid nano-PCM. Firstly, pure paraffin of 7 kg was melted in cylindrical vessel by using boiled water. Then, blend of  $\text{Al}_2\text{O}_3$  and  $\text{CuO}$  of predetermined quantities were added to liquified PCM, following the heating and mechanical agitation. The stirring proceeds for extra 30 minutes to prevent particle agglomeration and to attain well dispersion of nano powder through PCM. Afterward, the storage was layer by layer filled with the prepared compound.

It is worth mentioning that after pouring each layer, it was waited for around 30 minutes until complete freezing was attained. These steps were repeated until the whole annulus space was occupied with mixture. The aim behind this filling steps was to eliminate the growth of air bubbles inside the PCM throughout the freezing process. The test begins after one day of subjecting the storage to the controlled environment temperature at  $30^\circ\text{C}$  to achieve constant initial temperature of PCM.

### Numerical Simulation

#### Mathematical model

The enthalpy porosity technique, which is frequently used for modeling the PCM melting and freezing processes, is used to simulate phase transition in a TTHS. The

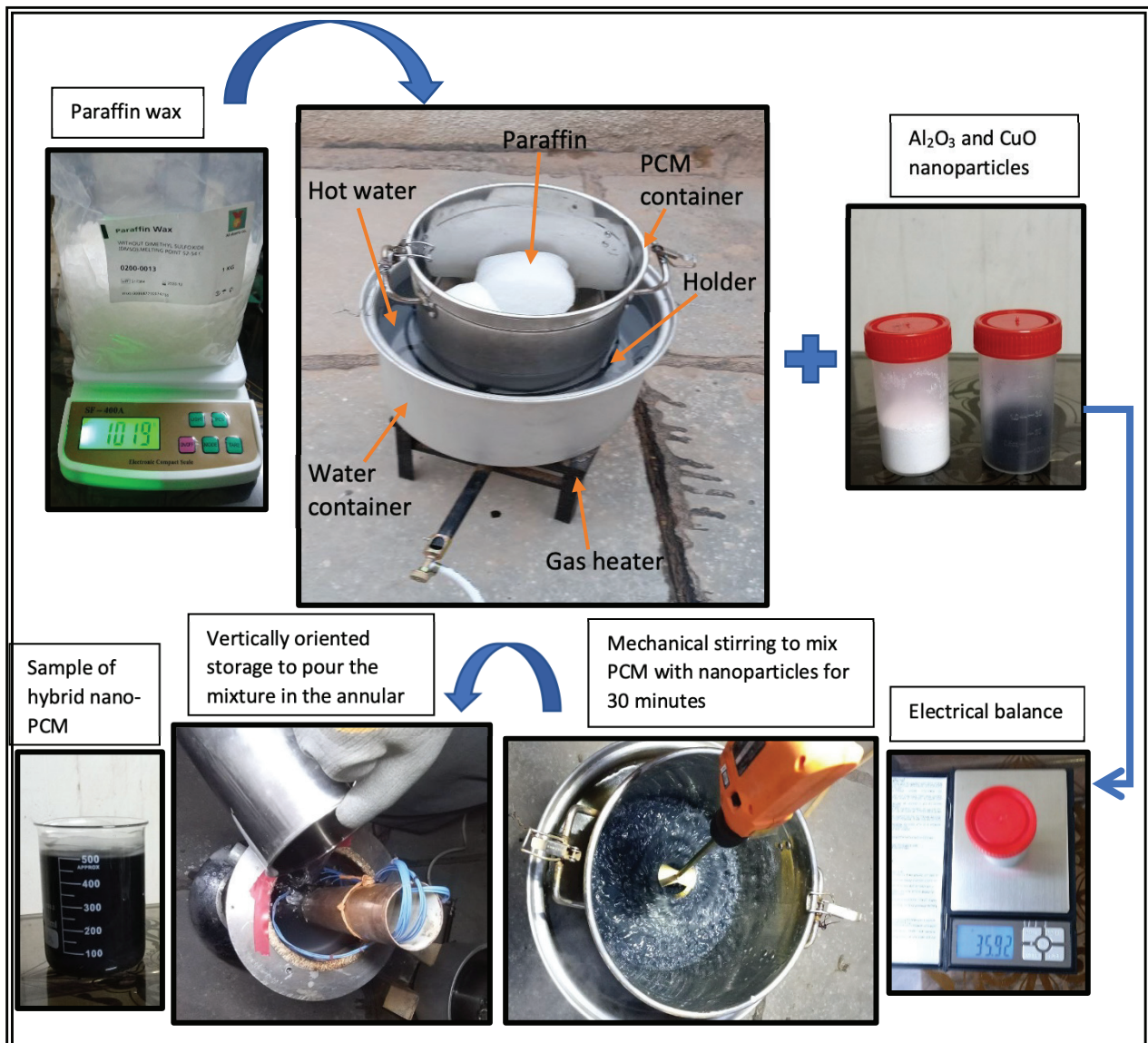


Figure 10. Hybrid nano-PCM preparation procedure.

mathematical model is discussed in the research [56,57] and is outlined in this subsection. The major characteristic of this approach is the representation of flow and latent heat in the mushy zone using appropriate source terms. According to Seddegh et al. [58], this approach has the following advantages: (i) Similarity between phase transition and the single-phase in term of the governing equations; (ii) at the solid–liquid interface, there are no specific conditions must be fulfilled. This implies that fixed grid solutions can be utilized; (iii) the enthalpy formulation includes the solution in a mushy zone between the two typical phases, involving solid and liquid phases; and (iv) tracking the interface between solid-liquid is easier with this method, which make numerical modeling simpler. However, the main limitation of enthalpy methods is the need of a temperature interval over which the latent heat is released and the phase transition takes place. This may be realistic for some phase change problems that involve a ‘mushy’ region, but not for others that have a constant transition temperature, such as ice freezing. Therefore, applying a temperature interval to these problems are non-physical assumption [59].

**Assumptions**

The following assumptions are used to simplify the mathematical model:

1. liquid state of PCM is considered as the Newtonian fluid.
2. Convection current of liquid PCM is laminar with no viscous dissipation.
3. All thermal characteristic of the paraffin depends on temperature except specific heat.
4. The Nano-PCM is homogeneous mixture.
5. The heat rejected to environment is negligible.
6. No-slip conditions between fluid and the boundaries.

**Governing equations**

Based on these arguments, the Navier-Stokes and energy equations were used to formulate the equations describing fluid motion and temperature distribution in the PCM become [58,60]:

Continuity equation:

$$\frac{\partial \rho_{hnpcm}}{\partial t} + \nabla \cdot (\rho_{hnpcm} \vec{V}) = 0 \tag{1}$$

Momentum equation:

$$\frac{\partial \vec{V}}{\partial t} + \vec{V} \cdot \nabla \vec{V} = \frac{1}{\rho_{hnpcm}} (-\nabla P + \mu_{hnpcm} \nabla^2 \vec{V} + (\rho\beta)_{hnpcm} \vec{g} (T - T_{ref})) + \vec{S} \tag{2}$$

Thermal energy equation:

$$\frac{\partial h}{\partial t} + \frac{\partial (\nabla H)}{\partial t} + \nabla \cdot (\vec{V} h) = \nabla \cdot \left( \frac{k_{hnpcm}}{(\rho C_p)_{hnpcm}} \nabla H \right) \tag{3}$$

The enthalpy of the material can be estimated as the sum of the sensible enthalpy (h) and the latent heat ( $\Delta H$ ) [61]:

$$H = h + \Delta H \tag{4}$$

Where

$$h = h_{ref} + \int_{T_{sef}}^T C_p dT \tag{5}$$

The reference enthalpy ( $h_{ref}$ ) is obtained at a reference temperature 273 K and  $C_p$  is the specific heat. The latent heat content can be written in terms of the latent heat of the material,  $L$ :

$$\Delta H = \lambda L \tag{6}$$

where  $\Delta H$  may vary from zero (solid) to  $L$  (liquid). Therefore, the liquid fraction,  $\lambda$ , can be defined as:

$$\lambda = \begin{cases} \frac{\Delta H}{L} = 0 & \text{if } T < T_{solidus} \\ \frac{\Delta H}{L} = 1 & \text{if } T > T_{liquidus} \\ \frac{\Delta H}{L} = \frac{T - T_{solidus}}{T_{liquidus} - T_{solidus}} & \text{if } T_{solidus} < T < T_{liquidus} \end{cases} \tag{7}$$

In Equation (2),  $\vec{S}$  is the Darcy’s law damping terms (as source term) that is implemented to the momentum equation due to phase change effects on convective heat transfer which is found as [62]:

$$\vec{S} = \frac{(1-\lambda)^2}{\lambda^3} A_{mush} \vec{V} \tag{8}$$

The coefficient  $A_{mush}$  is a mushy zone constant. This constant is a large number, usually  $10^5$ – $10^6$  [63]. In the current study  $A_{mush}$  is assumed constant and is assigned to  $10^6$ . To model the solidification process of the paraffin in the existing of  $Al_2O_3/CuO$  hybrid nanoparticles of different volume fraction, the subsequent relations were implemented to estimate the thermal characteristics of the hybrid nano-PCM.

The overall volume fraction of hybrid nanoparticles in the compound [64]

$$\varphi_{hnp} = \varphi_{np1} + \varphi_{np2} \tag{9}$$

Density of hybrid nano-PCM [65]:

$$\rho_{hnpcm} = \rho_{hnp} \varphi_{hnp} + (1 - \varphi_{hnp}) \rho_{pcm} \tag{10}$$

Where  $\rho_{hnp}$  is equivalent density of hybrid nanoparticles which presented in equation (11) [64]:

$$\rho_{hnp} = \frac{\varphi_{np1} \rho_{np1} + \varphi_{np2} \rho_{np2}}{\varphi_{hnp}} \tag{11}$$

Specific heat of hybrid nano-PCM [65]:

$$C_{p,hnpPCM} = \frac{C_{p,hnp}\rho_{hnp}\varphi_{hnp} + C_{p,pcm}\rho_{pcm}(1-\varphi_{hnp})}{\rho_{hnpPCM}} \quad (12)$$

Equivalent specific heat ( $C_{p,hnp}$ ) of hybrid nanoparticles can be calculated from equation (13) [64]:

$$C_{p,hnp} = \frac{\varphi_{np1}C_{p,np1}\rho_{np1} + \varphi_{np2}C_{p,np2}\rho_{np2}}{\rho_{hnpPCM}\varphi_{hnp}} \quad (13)$$

Viscosity of hybrid nano-PCM is estimated according to Batchelor model [66]:

$$\mu_{hnpPCM} = (1 + 2.5\varphi_{hnp} + 6.2(\varphi_{hnp})^2)\mu_{pcm} \quad (14)$$

Thermal conductivity of hybrid nano-PCM is obtained based on Maxwell model which can be used for low volume fraction [67]:

$$k_{hnpPCM} = \left( \frac{k_{hnp} + 2k_{pcm} + 2(k_{hnp} - k_{pcm})\varphi_{hnp}}{k_{hnp} + 2k_{pcm} - (k_{hnp} - k_{pcm})\varphi_{hnp}} \right) k_{pcm} \quad (15)$$

Equivalent thermal conductivity of hybrid nanoparticles ( $k_{hnp}$ ) is given as [64]:

$$k_{hnp} = \frac{(\varphi_{np1}k_{np1} + \varphi_{np2}k_{np2})}{\varphi_{hnp}} \quad (16)$$

Latent heat of fusion of hybrid nano-PCM [68,69]:

$$L_{hnpPCM} = \frac{L_{pcm}\rho_{pcm}(1-\varphi_{hnp})}{\rho_{hnpPCM}} \quad (17)$$

The subscript np1, np2, hnp, hnpPCM represent  $Al_2O_3$  nanoparticles, CuO nanoparticles, hybrid nanoparticles, and hybrid nano-PCM, respectively. Tables 1 and 2 summarizes the thermal characteristics of CuO/ $Al_2O_3$  nanoparticles and hybrid nano-PCM, respectively.

### Boundary conditions

To attain the liquid state of PCM at the beginning, the initial temperature was set to 70 °C, which is above the liquidus temperature. The type of “mass-flow-inlet” and “mass-flow-outlet” boundary conditions were respectively set for the HTF at the inlet and outlet of storage unit. HTF’s mass flow rates range between (3 kg/min – 12 kg/min), and its temperature changes from 30 to 40 °C. It is noteworthy that throughout the discharging process, inlet mass flow rate and inlet temperature of HTF were unchanged. As stated previously, the outer tube in the storage system is chosen as an adiabatic wall.

**Table 1.** Thermophysical properties of paraffin and nano-particles [70-72]

| Properties                    | Pure PCM  | $Al_2O_3$ | CuO        |
|-------------------------------|---|-----------|------------|
| Density (kg/m <sup>3</sup> )  | 750<br>$0.001(T - 319.15) + 1$                          | 3970 [72] | 6500 [70]  |
| Specific heat (J/kg °C)       | 2149  | 765 [70]  | 535.6 [70] |
| Thermal conductivity (w/m °C) | 0.21 if $T < T_{solidus}$<br>0.12 if $T > T_{liquidus}$ | 36 [71]   | 18 [71]    |
| Viscosity (pa.s)              | $0.001\exp\left(-4.25 + \frac{1790}{T}\right)$          | -         | -          |
| Latent heat of fusion (J/kg)  | 146700  | -         | -          |
| Solidus temperature, °C       | 52  | -         | -          |
| Liquidus temperature, °C      | 54  | -         | -          |

**Table 2.** Thermophysical properties of hybrid nano-PCM

| Properties                        | $\varphi = 0\%$ | $\varphi = 0.4\%$ | $\varphi = 0.8\%$ | $\varphi = 1.6\%$ | $\varphi = 3.2\%$ |
|-----------------------------------|-----------------|-------------------|-------------------|-------------------|-------------------|
| Density (kg/m <sup>3</sup> )      | 744.7           | 762.5             | 780.3             | 815.8299          | 886.87            |
| Specific heat (J/kg °C)           | 2149            | 2107.5            | 2068              | 1994.143          | 1864              |
| Thermal conductivity (S) (w/m °C) | 0.21            | 0.2133            | 0.21668           | 0.223583          | 0.238076          |
| Thermal conductivity (L) (w/m °C) | 0.12            | 0.1219            | 0.12385           | 0.127834          | 0.136199          |
| Viscosity (pa.s)                  | 0.003458        | 0.003622          | 0.003812          | 0.004266          | 0.0056406         |
| Latent heat of fusion (J/kg)      | 146700          | 142710            | 138901            | 131782            | 119255            |

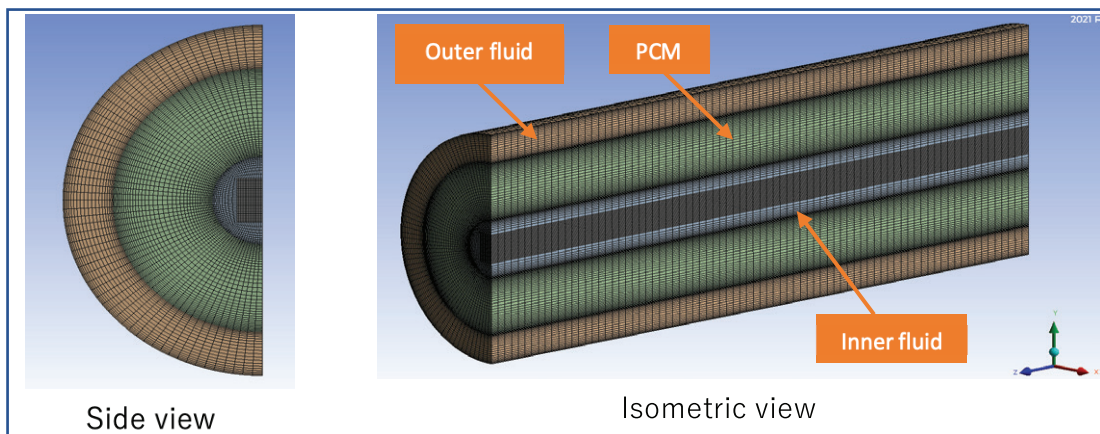


Figure 11. Grid generation for current case study.

Table 3. Mesh size and time period independency carried out on sample of hybrid nano-PCM

| Case | Number of elements | Number of nodes | Time step (s) | Freezing time (s) | Relative error (%) |
|------|--------------------|-----------------|---------------|-------------------|--------------------|
| 1    | 209670             | 218275          | 0.1           | 14731.54          | 5.83               |
| 2    | 307380             | 322595          | 0.1           | 14284.7           | 2.62               |
| 3    | 400530             | 415761          | 0.1           | 14120.45          | 1.44               |
| 4    | 307380             | 322595          | 0.01          | 13920             | -                  |
| 5    | 307380             | 322595          | 0.001         | 13844.83          | 0.54               |

### Mesh generation and independency study

To resolve the governing equations, a hexahedral uniform mesh was created (Fig. 11). High mesh density was generated near to tubes wall because of the higher velocity and temperature gradients adjacent to the heat transfer surface. The mesh and time independency tests were carried out to assign the required number of element and time interval. It was found that the case with 322595 elements, and 0.01 second time interval exhibit efficient solution stability and good accuracy with reasonable calculation time as seen in Table 3.

### Numerical procedure and validation

ANSYS FLUENT 21 were used to solve the aforementioned partial differential equations with the associated initial and boundary conditions. The software employs the enthalpy-porosity approach to model phase transition [73], where at each iteration, the liquid fraction for the PCM region is resolved using an enthalpy balance [74]. In this method, the mushy zone where both liquid and solid present was modeled as a “pseudo” porous medium with porosity equivalent to the liquid fraction. As PCM freezes, the porosity reduces from 1 (liquid) to 0 (solid). The SIMPLE algorithm outlined by Patankar [75] and the pressure-based solver were utilized to couple the velocity and pressure. The Navier-Stokes and energy equation terms were discretized using the QUICK method described by

Leonard [76]. The PRESTO scheme was chosen for pressure correction. The under-relaxation factors are 0.9, 1, 0.6, and 0.3 for liquid fraction, energy, momentum and pressure correction, respectively. To achieve solution stability in each case, the first-order implicit time-interval solving method is applied.

### Solution methods

As stated before, ANSYS FLUENT 21 based on enthalpy porosity model was used to simulate solidification process within hybrid nano-PCM. It includes the subsequent steps:

- Generate mesh for the physical domain, which was detailed in section 3.5.
- Implementing the governing equations of continuity, momentum, and thermal energy of hybrid nano-PCM on control volume and produce group of differential equations containing velocity, temperature, enthalpy of formulation and other variables [77].
- Convert set of differential equations into solvable algebraic equations by using finite volume method. This process named discretization approach [78].
- Solve the discretized equations for each control volume iteratively.

### Convergence criteria

Error residuals, which explicitly indicate the error in the solution of the system of equations, are the popular

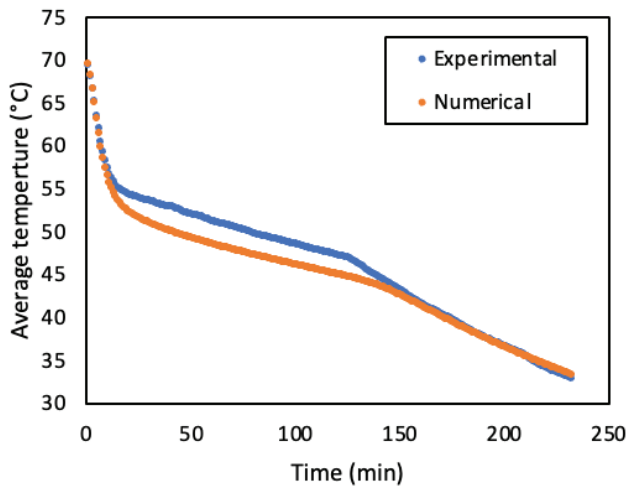


**Figure 12.** Comparison of average temperature between the experimental and numerical result.

method for determining solution convergence. Thus, every solved equation will have its own magnitude of residual for each cell in the model. When the residuals are attained to a certain level, the solution is considered to have converged [79]. This level of residual is  $10^{-3}$  for all variables except the residual of energy equation, which should be kept less than  $10^{-6}$  [80]. In this study, the predetermined convergences criteria are  $10^{-5}$  for each velocity and continuity equations while  $10^{-7}$  for energy equation. Since all cases of present study are transient, this order of residual was satisfied for each time step during calculation by providing 50 maximum iterations per time step and 2,000,000 maximum numbers of time steps.

Generally, to approach convergence for each 3-D model, it requires around 6,000,000 total iterations. This complex problem may take around (13) days of calculations for each case by using high performance computer of the following specifications: Desktop of AMD Ryzen 5900X 12- Core - (4.6) GHz processor with water cooler, RAM: 32 GB, Hard: 932 GB and Graphic card: NVIDIA GeForce GTX-1050.

### Validation

To evaluate the validity of the current numerical data, the PCM average temperature that acquired from the numerical modeling is verified with corresponding experimental result. The Figure 12 shows the time-dependent temperature profile (numerical and experimental) for 0.4% volume fraction, 30 °C HTF inlet temperature and 3 kg/min mass flow rate. As depicted in Figure 12, a slight deviation, lower than about 4% in average, can be noticed between the numerical and experimental outcomes, exhibiting an acceptable reliability of the solidification simulation.

## RESULTS AND DISCUSSION

### Visualization of the Solidification Process

The discharging begins with the PCM entirely melted as result of the earlier melting process, whereas the water is flowing at a temperature less than the solidification temperature of the base PCM. This causes solidification to begin from inner and intermediate surfaces, resulting in the creation of a small solidified layer next to each surface. This layer increases steadily by transferring heat through the surfaces to the water surrounding the annulus. The temperature contour and streamline during solidification are demonstrated in Figure 13.

In the preliminary stages, the heat transfer that takes place between the cold wall (intermediate and inner tube) and liquid zone of PCM causes a temperature variation. This variation produces the buoyancy force, which gradually overcomes the viscous resistance and contributes to the production of a buoyancy driving force in the molten portion of the PCM. During this period ( $t = 10$  min) convection current has become the major heat transmission mode and acts as an extra provide of heat release from the liquid PCM, leading to more rapid solidification in subsequent times ( $t=45$  min, 90 min and 135 min). In the meantime, the annulus is mostly dominated by the liquid phase. After 45 min from the starting of the solidification process, a single vortex located at lower portion and two major vortices located near to tubes. one adjacent to the intermediate tube and one near to inner tube. At  $t=90$  min, the associated isotherms have the appearance of deformed loops existing throughout the entire annulus. Afterward ( $t=135$  min), PCM at the lower part of the annulus has been mostly solidified while the PCM at the upper has been partially solidified. The remaining liquid region that located between solid PCM layers needed further duration to solidify because the thermal resistance rose as the solid layers near to the surface increased. Comparing solidification of PCM at time of 135 min and 180 min, obviously illustrate that the isotherms travel upward at a slow rate in the upper part of the annulus and there are two small vortices exist in the upper part of annulus. This solidification characteristic implies that free convection is still the primary heat transfer mode at the upper portion of annulus, whereas conduction heat transfer governs solidification at the lower portion of the annulus. After the period of 180 min, isotherms make an elongated oval configuration. The vertices decrease in both strength and size until they vanish when the whole PCM solidified at 225 min. The superiority of conduction over convection can be determined when the vortices structure collapses and temperature contour begin to be uniformly distributed which occur after 180 min of freezing period.

### Effect of Mass Flow Rate

The effect of varying the HTF mass flow rate (3, 6, 9 and 12 kg/min) on the solidification process was assessed at 30

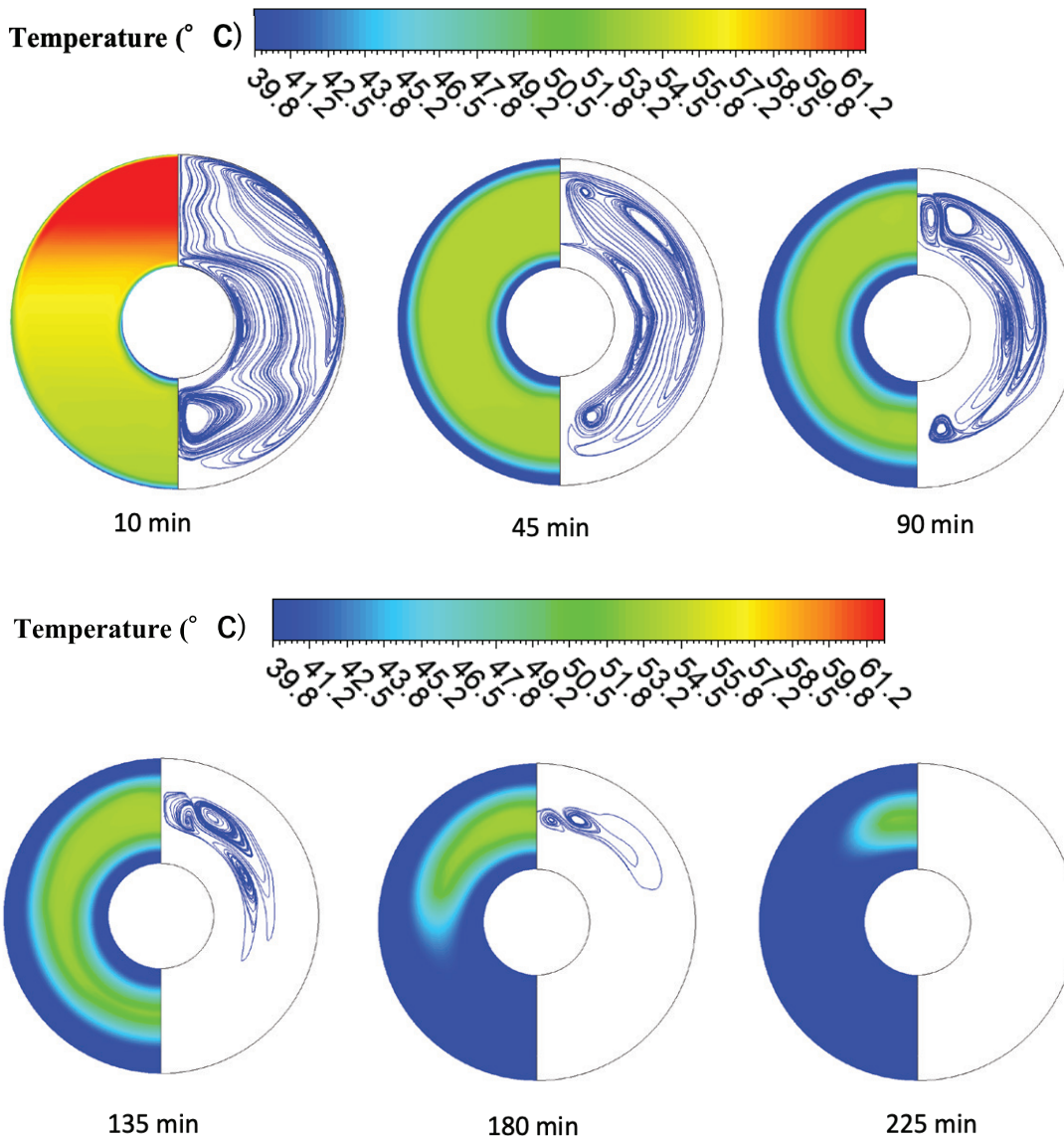


Figure 13. Isotherms (Left) and streamline (Right) over time for Pure PCM.

°C of HTF inlet temperature. Figure 14 and Figure 15 illustrate time wise variation of average PCM temperature and liquid fraction, respectively. At a given time, higher mass flow rate, lower average temperature of PCM and lower liquid fraction (higher amount of solidified PCM). This is because high mass flow rate causes high heat transfer coefficient in tube and outer shell side and thus higher heat rate into PCM. The percentage reduction of solidification time is 4.85%, 7.28% and 8.5 % for mass flow rate of 6, 9 and 12 kg/min respectively compare to mass flow rate of 3 kg/min, see Figure 16. The decrease in solidification duration is minor with boost mass flow rate. Thus, the total solidification time is not significantly affected by an increase in mass flow rate. With higher mass flow rates, the HTF has a

shorter residence duration and the heat transfer surface of the HTF tube practically remains isothermal.

It is worth to consider that decreasing solidification time has some implications on the system design and performance of storage system as follow: (i) a shorter solidification time indicates that the storage unit can be discharged faster, which can enhance the unit efficiency; (ii) a shorter solidification time can promote the storage system to respond quickly to the fluctuating demand or supply of thermal energy, which is useful for integrating the system with renewable energy sources and improving load management; and (iii) a shorter solidification time also implies that the storage device can be designed with a smaller volume or a lower amount of PCM, which can minimize the system cost and weight.

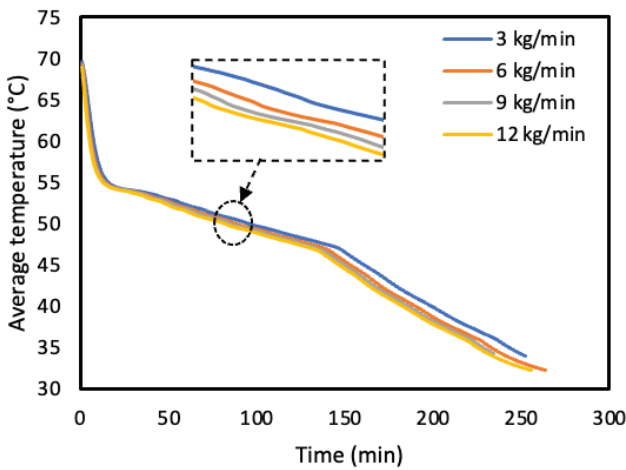


Figure 14. Average PCM temperature over time for various mass flow rate.

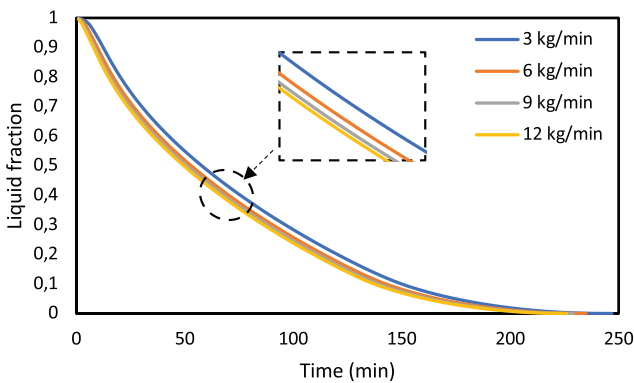


Figure 15. Time wise variation of liquid fraction for different mass flow rate.

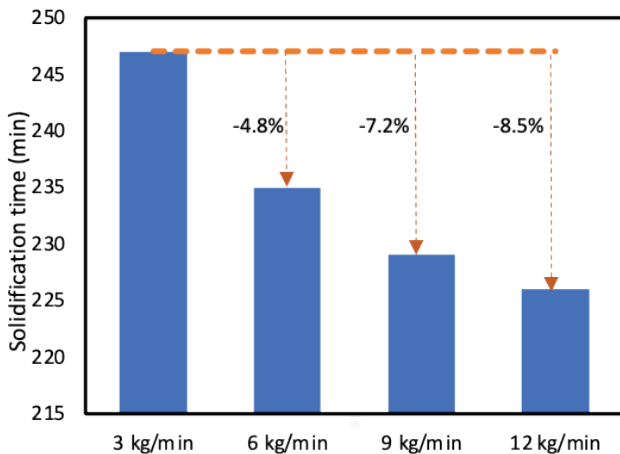


Figure 16. Total solidification time for different mass flow rate.

Effect of Inlet Temperature

To study the effect of inlet temperature on the freezing processes, Figure 17 and Figure 18 depict average temperature and liquid fraction of the PCM freezing under various inlet temperature of 30, 35, and 40 °C. The freezing rate enhanced as the inlet temperature decreased, ascribed to the augmentation in the heat transfer. It is noticed that the time required to approach to 50 °C is 125, 179 and 216 min respectively for HTF inlet temperatures of 30, 35 and 40 °C. The solidification time is considerably decrease even with a 5 °C reduction of the HTF inlet temperature. This is because the lower HTF temperature enhance the potential temperature gradient between PCM and HTF temperature which in turn intensify the heat transfer rate. Moreover, higher temperature difference between PCM and HTF lead to enhance buoyancy effects which promote convection currents. Similar observations were mentioned by [81]. The total solidification time can be reduced up to 38% when inlet temperature decreases from 40 to 30 °C, see Figure 19. This indicate that decrease in inlet fluid temperature has a greater impact on heat transfer intensification than an increase in HTF mass flow rate.

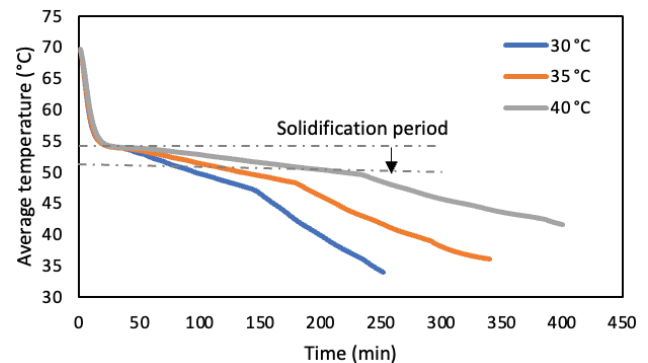


Figure 17. Average PCM temperature vs time for different HTF inlet temperature.

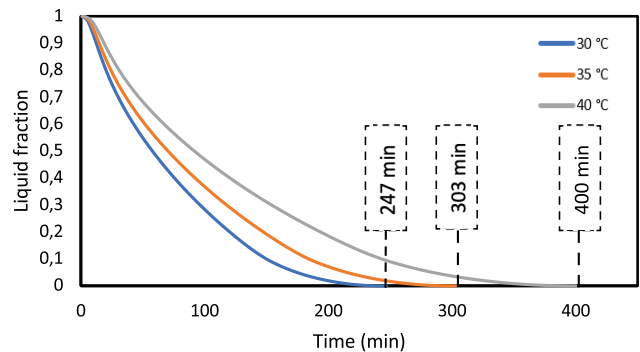
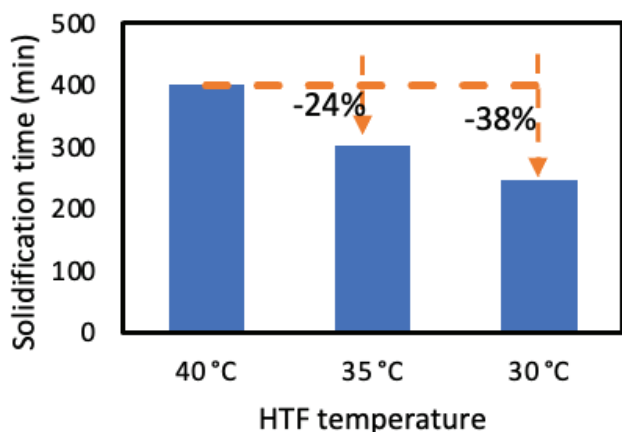


Figure 18. Liquid fraction for different HTF inlet temperature.



**Figure 19.** Total solidification time for different HTF inlet temperature.

### Effect of Inclusion Hybrid Nanoparticle

Figures 20-23 demonstrate the impact of mixing  $\text{Al}_2\text{O}_3/\text{CuO}$  hybrid nanopowder on average temperature of PCM, temperature distribution, liquid-fraction contours, and velocity vectors over varying solidification periods. Results reveal that raising the concentration of hybrid Nano powder enhances the rate of heat transmission and, as a result, reduces the time required for fully freezing. This is because the addition of nanoparticles boosts the thermal conductivity and viscosity of the mixture. Increasing viscosity cause shear force increase between fluid layers, which resist free convection current and reduces the temperature gradient. In fact, if the enhancement in thermal conductivity is higher than the reduction in temperature gradient, the nano-PCM reject more heat and solidifies faster. This scenario is observed for all nanoparticle concentration taken in this investigation. The improvement in heat transfer can be noticed from decreasing the PCM average temperature with increase nano concentration in Figure 20. Significant differences in average PCM temperature are obtained at the final stage of discharging. Figure 21 manifests that inclusion nanoparticles delay conduction superiority and maximizes convection contribution, causing the isotherms to appear more distorted and less crowded. This can be seen in hybrid nano-PCM ( $\phi = 0.4\%$ , 0.8%, 1.6% and 3.2%) as compare to pure PCM throughout all the solidification duration. Figure 22 shows little difference in solid-liquid interface's configuration between the pure PCM case and hybrid nano-PCM cases during the last stages of solidification, when heat transfer is primarily by conduction. In fact, the variations are more obvious throughout the initial stages (e.g., 10 min) because of convection superiority, However the contour lines appear more deformed in comparison to those of pure PCM case.

Concerning velocity field, Figure 23 demonstrates that the velocity magnitude at the upper portion of

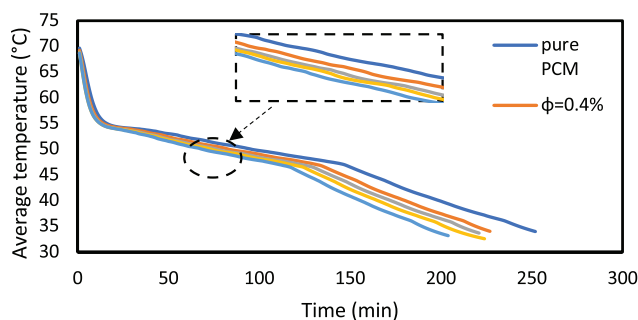


**Figure 20.** Average PCM temperature vs time for different nanoparticle concentration.

annulus is higher than lower portion, ascribing to buoyancy effect which induce high convection current at upper portion of annulus. When hybrid nanoparticles are implemented to the pure PCM, the velocity values (red color region, for instance) diminish, implying a decrease in convection current of liquid PCM inside the annulus. Furthermore, when comparing the pure PCM to the nano-PCM, the distribution of velocity vectors seems more packed in the top zone. this indicate that the existence of nanoparticles resists the movement of liquid PCM over the initial stage (10 min and 45 min) of discharging in which convection is dominant mode. This scenario is not true in subsequent solidification stages because of the evolving dominance of conduction over convection as time passes. The rise in nanoparticle concentration causes a slight drop in flow velocity during the last periods of solidification (90 min and 135 min., Figure 21). This is due to the viscosity rise of PCM-melt with adding  $\text{Al}_2\text{O}_3/\text{CuO}$  hybrid nanoparticles. Generally, the effect of nanoparticles on average PCM temperature, isotherms, liquid-fraction contours and velocity vectors becomes more pronounced as volume concentration boost and/or time passes.

Temporal variations of the liquid fraction of hybrid nano-PCM throughout the freezing process at 30 °C inlet temperature and 3 kg/min mass flow rate are depicted in Figure 24. According to the figure, the addition of  $\text{Al}_2\text{O}_3/\text{CuO}$  nanoparticles with concentration 0.4%, 0.8%, 1.6% and 3.2% does not initially display a considerable difference, however over the time, a significant reduction of liquid fraction is observed as compared to the pure paraffin. The percentages of overall time reduction of nano-PCM in comparison to the comparable values in the case with pure PCM are listed in Table 4. The pure PCM requires 247 min to fully freeze. In comparison to pure PCM case, nano-PCM with concentration of 0.4%, 0.8%, 1.6% and 3.2% needs less duration and leads in overall time savings of 10.9%, 14.1%, 17.8% and 23.8%, respectively.

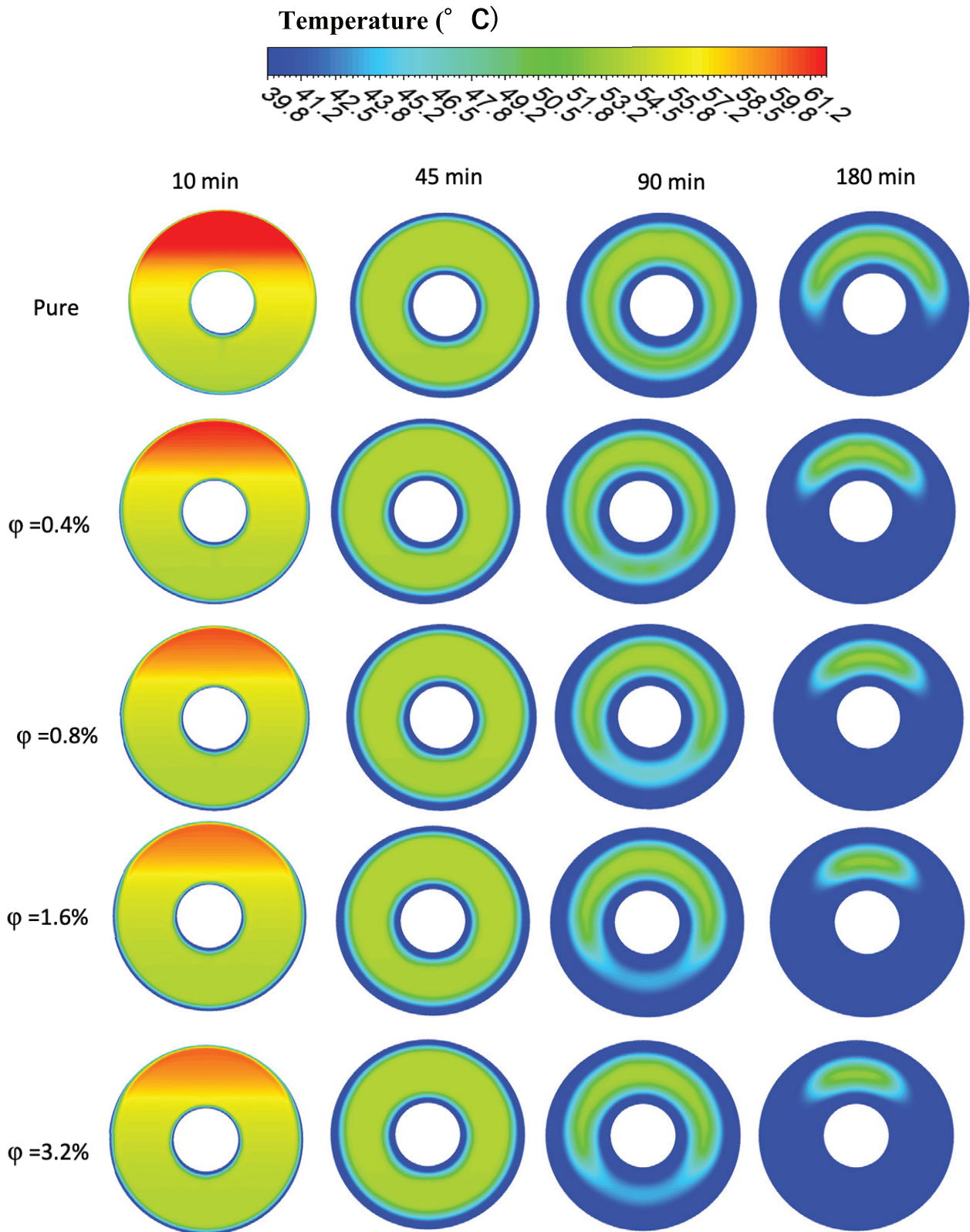


**Figure 21.** Temperature contour for various volume fraction of nanoparticles at HTF inlet temperature of 30 °C and mass flow rate of 3 kg/min.

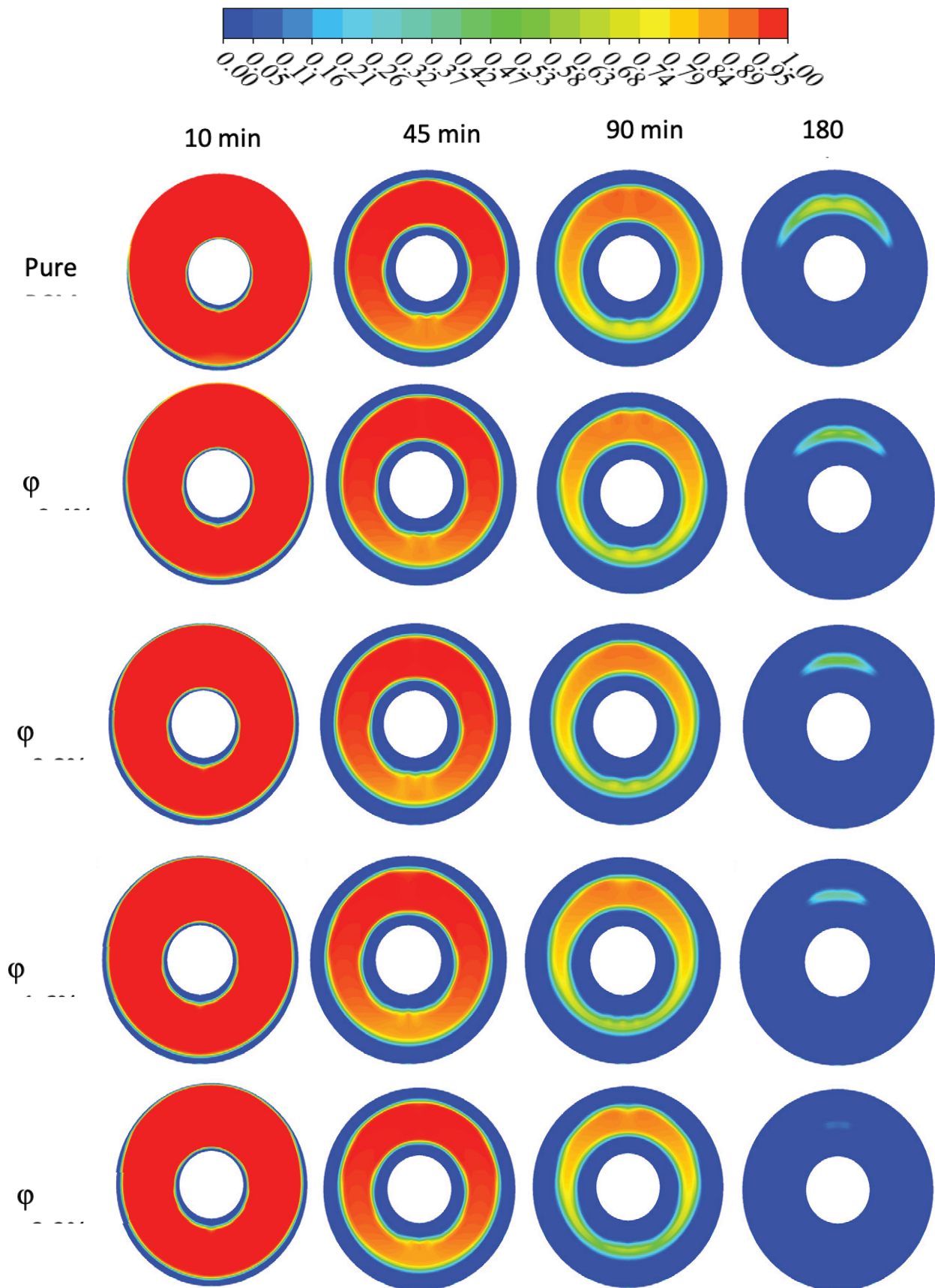
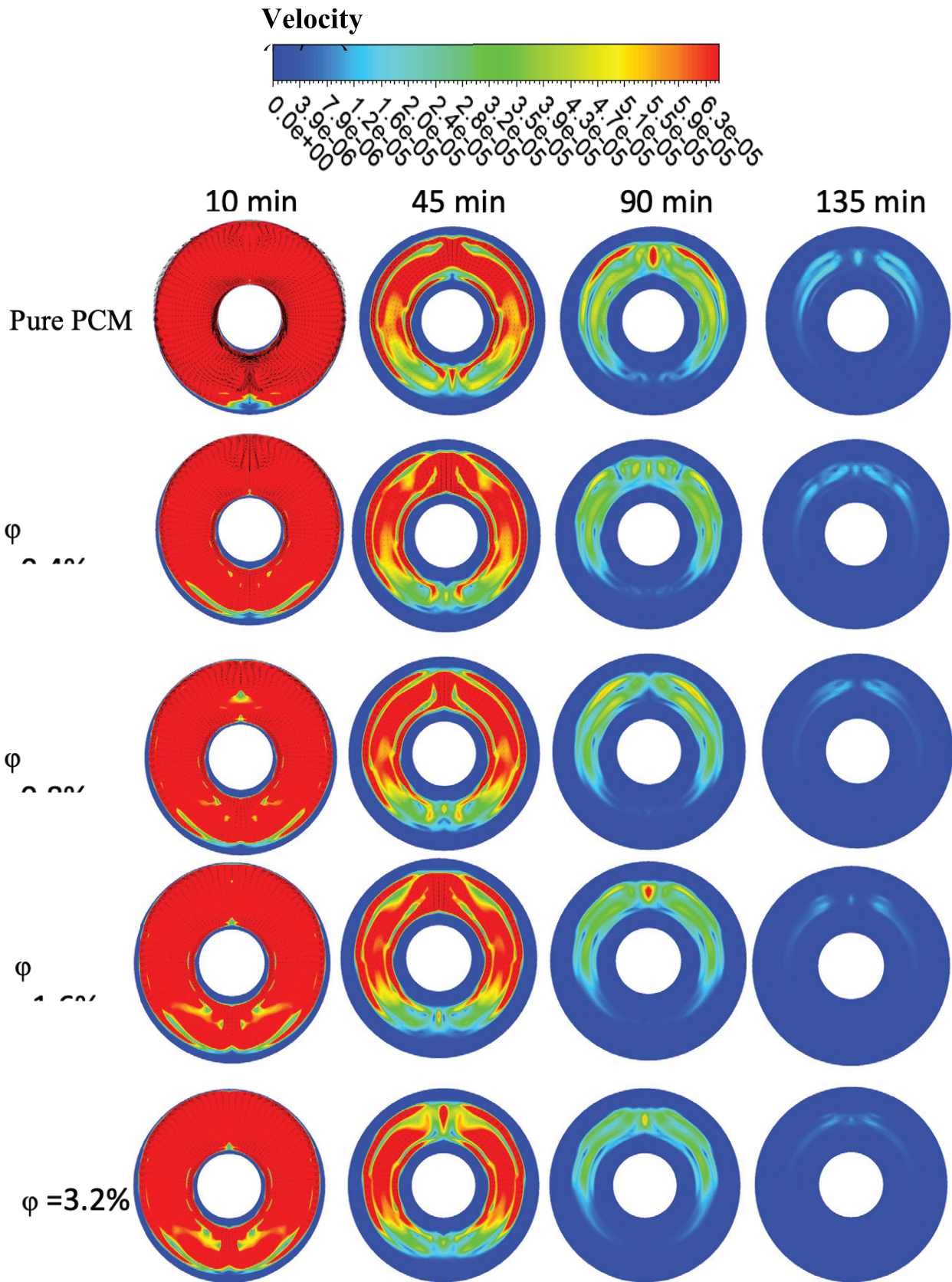
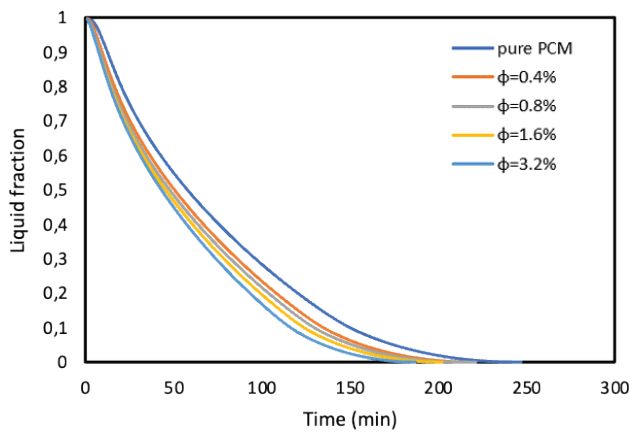


Figure 22. Time evolution liquid fraction for different nanoparticle concentration.



**Figure 23.** Tangential velocity vector at different duration and nano concentration throughout discharging of nano-PCM at  $T_{HTF} = 30\text{ }^{\circ}\text{C}$ .



**Figure 24.** Temporal variation of liquid fraction for different nanoparticle volume fraction.

**Table 4.** Influence of hybrid nanoparticles concentration on solidification time at HTF 30 °C

| Concentration % | Time (min) | Time reduction % |
|-----------------|------------|------------------|
| 0               | 247        | 0.0              |
| 0.4             | 220        | 10.93            |
| 0.8             | 212        | 14.17            |
| 1.6             | 203        | 17.81            |
| 3.2             | 188        | 23.88            |

## CONCLUSION

The influence of employing paraffin equipped with Al<sub>2</sub>O<sub>3</sub>/CuO hybrid nano on the thermal performance of triplex tube heat storage (TTHS) was analyzed and compared to pure paraffin (TTHS). The experimental and numerical studies were carried out at various inlet temperature (30, 35 and 40 °C) and mass flow rate (3, 6, 9 and 12 kg/min). The subsequent major findings are obtained from this investigation:

1. Heat transfer and consequently discharging period are directly proportional to the inlet temperature of the HTF. The present research manifests that decrease the inlet HTF temperature from 40 °C to 30 °C can save total discharging duration by 38%.
2. The rate of solidification is more affected by HTF inlet temperature than by mass flow rate.
3. As the mass flow rate booted from 3 kg/min to 12 kg/min, the overall discharging duration reduced by 8.5%.
4. PCM with hybrid nano-additives concentration of 0.4%, 0.8%, 1.6%, and 3.2% can respectively save overall discharging period by 10.9%, 14.1%, 17.8%, and 23.8%.
5. The variation in average PCM temperature, isotherms, liquid-fraction and velocity value becomes increasingly

noticeable as time evolves and/or the volume concentration increase.

## NOMENCLATURE

|            |                                   |
|------------|-----------------------------------|
| PCM        | Phase change material             |
| TTHS       | Triplex tube heat storage         |
| HTF        | Heat transfer fluid               |
| AlN        | aluminium nitride                 |
| GNP        | graphene nano-platelets           |
| DSC        | Differential scanning calorimetry |
| $\vec{V}$  | Fluid velocity (m/sec)            |
| $P$        | Pressure (pa)                     |
| $\vec{g}$  | Gravity (m/sec <sup>2</sup> )     |
| $T$        | Temperature (°C)                  |
| $\vec{S}$  | Darcy's law damping term          |
| $t$        | Time                              |
| $h$        | sensible enthalpy                 |
| $\Delta H$ | Latent heat content               |
| $C_p$      | Specific heat (J/kg °C)           |
| $L$        | Latent heat of fusion (J/kg)      |
| $k$        | Thermal conductivity (w/m °C)     |
| $H$        | Enthalpy of material (J /kg)      |

### Greek symbols

|           |                                |
|-----------|--------------------------------|
| $\rho$    | Density (kg/m <sup>3</sup> )   |
| $\mu$     | Fluid viscosity (pa.s)         |
| $\beta$   | Thermal expansion factor (1/K) |
| $\lambda$ | Liquid fraction                |
| $\varphi$ | Volume fraction                |

### Subscripts

|       |                                   |
|-------|-----------------------------------|
| npcm  | Nano-phase change material        |
| hnpcm | Hybrid nano phase change material |
| ref   | Reference value                   |
| np1   | Aluminum oxide nanoparticles      |
| np2   | Copper oxide nanoparticles        |
| hnp   | Hybrid nanoparticles              |
| mush  | Mushy                             |

## AUTHORSHIP CONTRIBUTIONS

Authors equally contributed to this work.

## DATA AVAILABILITY STATEMENT

The authors confirm that the data that supports the findings of this study are available within the article. Raw data that support the finding of this study are available from the corresponding author, upon reasonable request.

## CONFLICT OF INTEREST

The author declared no potential conflicts of interest with respect to the research, authorship, and/or publication of this article.

## ETHICS

There are no ethical issues with the publication of this manuscript.

## REFERENCES

- [1] Dincer I, Rosen MA. Thermal Energy Storage: Systems and Applications. John Wiley & Sons; 2021. [\[CrossRef\]](#)
- [2] Afsharpanah F, Pakzad K, Ajarostaghi SSM, Arıcı M. Assessment of the charging performance in a cold thermal energy storage container with two rows of serpentine tubes and extended surfaces. *J Energy Storage* 2022;51:104464. [\[CrossRef\]](#)
- [3] Khudhair A, Hatem F, Mohammed Ridha D. Enhancement of thermal storage properties of phase change material by using metallic swarf. *Eng Technol J* 2018;36:586–595. [\[CrossRef\]](#)
- [4] Abed AH. Thermal storage efficiency enhancement for solar air heater using a combined SHSm and PCM cylindrical capsules system: Experimental investigation. *Eng Technol J* 2016;34:999–1011. [\[CrossRef\]](#)
- [5] Tawalbeh M, Khan HA, Al-Othman A, Almomani F, Ajith S. A comprehensive review on the recent advances in materials for thermal energy storage applications. *Int J Thermofluids* 2023;18:100326. [\[CrossRef\]](#)
- [6] Aljabair S, Alesbe I, Ibrahim SH. Review on latent thermal energy storage using phase change material. *J Therm Eng.* 2021;9:247–256. [\[CrossRef\]](#)
- [7] Sadr AN, Shekaramiz M, Zarinfar M, Esmaily A, Khoshtarash H, Toghraie D. Simulation of mixed-convection of water and nano-encapsulated phase change material inside a square cavity with a rotating hot cylinder. *J Energy Storage* 2022;47:103606. [\[CrossRef\]](#)
- [8] Modi N, Wang X, Negnevitsky M. Solar hot water systems using latent heat thermal energy storage: perspectives and challenges. *Energies* 2023;16:1969. [\[CrossRef\]](#)
- [9] Romdhane SB, Amamou A, Khalifa RB, Said NM, Younsi Z, Jemni A. A review on thermal energy storage using phase change materials in passive building applications. *J Build Engineer* 2020;32:101563. [\[CrossRef\]](#)
- [10] Munir Z, Roman F, Niazi BMK, Mahmood N, Munir A, Hensel O. Thermal analysis of a solar latent heat storage system using Scheffler concentrator for agricultural applications. *Appl Therm Engineer* 2023;218:119230. [\[CrossRef\]](#)
- [11] Raut D, Lanjewar S, Kalamkar VR. Effect of geometrical and operational parameters on paraffin's melting performance in helical coiled latent heat storage for solar application: a numerical study. *Int J Therm Sci* 2022;176:107509. [\[CrossRef\]](#)
- [12] Yang S, Shao XF, Luo JH, Oskouei SB, Bayer Ö, Fan LW. A novel cascade latent heat thermal energy storage system consisting of erythritol and paraffin wax for deep recovery of medium-temperature industrial waste heat. *Energy* 2023;265:126359. [\[CrossRef\]](#)
- [13] Sadr AK, Sivan S, Midhun V, Behera SR. Experimental and numerical investigation of solid-solid phase change material assisted heat sink with integrated heat pipe for electronic cooling. *J Energy Storage* 2023;59:106494. [\[CrossRef\]](#)
- [14] Rathore PKS, Gupta NK, Yadav D, Shukla SK, Kaul S. Thermal performance of the building envelope integrated with phase change material for thermal energy storage: An updated review. *Sustain Cities Soc* 2022;79:103690. [\[CrossRef\]](#)
- [15] Paul J, Pandey A, Mishra YN, Said Z, Mishra YK, Ma Z, et al. Nano-enhanced organic form stable PCMs for medium temperature solar thermal energy harvesting: Recent progresses, challenges, and opportunities. *Renew Sustain Energy Rev* 2022;161:112321. [\[CrossRef\]](#)
- [16] Chang Y, Yao X, Chen Y, Zou D. Review on ceramic-based composite phase change materials: preparation, characterization and application. *Compos Part B Engineer* 2023;110584. [\[CrossRef\]](#)
- [17] Safari V, Abolghasemi H, Darvishvand L, Kamkari B. Thermal performance investigation of concentric and eccentric shell and tube heat exchangers with different fin configurations containing phase change material. *J Energy Storage* 2021;37:1–17. [\[CrossRef\]](#)
- [18] Sodhi GS, Muthukumar P. Compound charging and discharging enhancement in multi-PCM system using non-uniform fin distribution. *Renew Energy* 2021;171:299–314. [\[CrossRef\]](#)
- [19] Ebrahimi A, Hosseini MJ, Ranjbar AA, Rahimi M, Bahrampoury R. Melting process investigation of phase change materials in a shell and tube heat exchanger enhanced with heat pipe. *Renew Energy* 2019;138:378–394. [\[CrossRef\]](#)
- [20] Ling YZ, Zhang XS, Wang F, She XH. Performance study of phase change materials coupled with three-dimensional oscillating heat pipes with different structures for electronic cooling. *Renew Energy* 2020;154:636–649. [\[CrossRef\]](#)
- [21] Haddad Z, Iachachene F, Sheremet MA, Abu-Nada E. Numerical investigation and optimization of melting performance for thermal energy storage system partially filled with metal foam layer: New design configurations. *Appl Therm Engineer* 2023;223:119809. [\[CrossRef\]](#)
- [22] Righetti G, Zilio C, Longo GA, Hooman K, Mancin S. Experimental study on the effect of metal foams pore size in a phase change material based thermal energy storage tube. *Appl Therm Engineer* 2022;217:119163. [\[CrossRef\]](#)
- [23] Singh SK, Verma SK, Kumar R. Thermal performance and behavior analysis of SiO<sub>2</sub>, Al<sub>2</sub>O<sub>3</sub> and

- MgO based nano-enhanced phase-changing materials, latent heat thermal energy storage system. *J Energy Storage* 2022;48:103977. [CrossRef]
- [24] Nie C, Deng S, Liu J, Rao Z. Performance evaluation of shell-tube latent heat storage unit using nanoparticles with cascaded concentration. *J Energy Storage* 2023;62:106892. [CrossRef]
- [25] Yu X, Tao Y. Improvement of thermal cycle stability of paraffin/expanded graphite composite phase change materials and its application in thermal management. *J Energy Storage* 2023;63:107019. [CrossRef]
- [26] Tang X, Zhang J, Wang J, Xu T, Du Y, Fan G, et al. Preparation and application of paraffin/expanded graphite-based phase change material floor for solar-heat pump combined radiant heating systems. *ACS Sustain Chem Engineer* 2023;11:2871–2884. [CrossRef]
- [27] Fikri MA, Pandey A, Samykano M, Kadirgama K, George M, Saidur R, et al. Thermal conductivity, reliability, and stability assessment of phase change material (PCM) doped with functionalized multi-wall carbon nanotubes (FMWCNTs). *J Energy Storage* 2022;50:104676. [CrossRef]
- [28] Li X, Zhao Y, Min X, Xiao J, Wu X, Mi R, et al. Carbon nanotubes modified graphene hybrid aerogel-based composite phase change materials for efficient thermal storage. *Energy Build* 2022;273:112384. [CrossRef]
- [29] Cabeza LF, Zsembinszki G, Martín M. Evaluation of volume change in phase change materials during their phase transition. *J Energy Storage* 2020;28:101206. [CrossRef]
- [30] Magendran SS, Khan FSA, Mubarak NM, Vaka M, Walvekar R, Khalid M, et al. Synthesis of organic phase change materials (PCM) for energy storage applications: A review. *Nano-Struct Nano-Objects* 2019;20:100399. [CrossRef]
- [31] Mahdi JM, Nsofor EC. Solidification enhancement of PCM in a triplex-tube thermal energy storage system with nanoparticles and fins. *Appl Energy* 2018;211:975–986. [CrossRef]
- [32] Liu MJ, Fan LW, Zhu ZQ, Feng B, Zhang HC, Zeng Y. A volume-shrinkage-based method for quantifying the inward solidification heat transfer of a phase change material filled in spherical capsules. *Appl Therm Engineer* 2016;108:1200–1205. [CrossRef]
- [33] Ismail M, Alkhazaleh AH, Masri J, Ali AM, Ali M. Experimental and numerical analysis of paraffin waxes during solidification inside spherical capsules. *Therm Sci Engineer Prog* 2021;26:101095. [CrossRef]
- [34] Chen L, Wang L, Wang Y, Chen H, Lin X. Influence of phase change material volume shrinkage on the cyclic process of thermal energy storage: A visualization study. *Appl Therm Engineer* 2022;203:117776. [CrossRef]
- [35] Abdulateef AM, Mat S, Abdulateef J, Sopian K, Al-Abidi AA. Geometric and design parameters of fins employed for enhancing thermal energy storage systems: A review. *Renew Sustain Energy Rev* 2018;82:1620–1635. [CrossRef]
- [36] Karami R, Kamkari B. Experimental investigation of the effect of perforated fins on thermal performance enhancement of vertical shell and tube latent heat energy storage systems. *Energy Conver Manage* 2020;210:112679. [CrossRef]
- [37] Khan LA, Khan MM. Role of orientation of fins in performance enhancement of a latent thermal energy storage unit. *Appl Therm Engineer* 2020;175:115408. [CrossRef]
- [38] Yousef MS, Hassan H, Kodama S, Sekiguchi H. An experimental study on the performance of single slope solar still integrated with a PCM-based pin-finned heat sink. *Energy Procedia* 2019;156:100–104. [CrossRef]
- [39] Liu Z, Liu Z, Guo J, Wang F, Yang X, Yan J. Innovative ladder-shaped fin design on a latent heat storage device for waste heat recovery. *Appl Energy* 2022;321:119300. [CrossRef]
- [40] Wu J, Li N, Wu Z. Experimental investigation of latent energy storage systems with the tree-pin-shaped fin. *Appl Therm Engineer* 2023;227:120370. [CrossRef]
- [41] Mahdi JM, Nsofor EC. Multiple-segment metal foam application in the shell-and-tube PCM thermal energy storage system. *J Energy Storage* 2018;20:529–541. [CrossRef]
- [42] Hamza N, Aljabair S. Review of heat transfer enhancement using hybrid nanofluid or twisted tape insert. *J Mech Engineer Res Dev* 2021;44:345–357.
- [43] Khan Z, Khan ZA, Sewell P. Heat transfer evaluation of metal oxides based nano-PCMs for latent heat storage system application. *Int J Heat Mass Transf* 2019;144:118619. [CrossRef]
- [44] Hosseinizadeh SF, Darzi AAR, Tan FL. Numerical investigations of unconstrained melting of nano-enhanced phase change material (NEPCM) inside a spherical container. *Int J Therm Sci* 2012;51:77–83. [CrossRef]
- [45] Al-Jethelah M, Tasnim SH, Mahmud S, Dutta A. Melting of nano-PCM in an enclosed space: Scale analysis and heatline tracking. *Int J Heat Mass Transf* 2018;119:841–859. [CrossRef]
- [46] Ebadi S, Tasnim SH, Aliabadi AA, Mahmud S. Melting of nano-PCM inside a cylindrical thermal energy storage system: Numerical study with experimental verification. *Energy Conver Manage* 2018;166:241–259. [CrossRef]
- [47] Murugan P, Ganesh Kumar P, Kumaresan V, Meikandan M, Malar Mohan K, Velraj R. Thermal energy storage behaviour of nanoparticle enhanced PCM during freezing and melting. *Phase Transitions* 2018;91:254–270. [CrossRef]

- [48] Karaipekli A, Biçer A, Sarı A, Tyagi VV. Thermal characteristics of expanded perlite/paraffin composite phase change material with enhanced thermal conductivity using carbon nanotubes. *Energy Convers Manage* 2017;134:373–381. [CrossRef]
- [49] Gorzin M, Hosseini MJ, Rahimi M, Bahrampoury R. Nano-enhancement of phase change material in a shell and multi-PCM-tube heat exchanger. *J Energy Storage* 2019;22:88–97. [CrossRef]
- [50] Hamza N, Aljabair S. Numerical and experimental investigation of heat transfer enhancement by hybrid nanofluid and twisted tape. *Eng Technol J* 2022;41:69–85. [CrossRef]
- [51] Khan Z, Khan ZA. Experimental and numerical investigations of nano-additives enhanced paraffin in a shell-and-tube heat exchanger: A comparative study. *Appl Therm Engineer* 2018;143:777–790. [CrossRef]
- [52] Hamali W, Almusawa MY. Transient heat transfer of NEPCM during solidification using Galerkin method. *Case Stud Therm Engineer* 2022;35:102114. [CrossRef]
- [53] Rothan YA. Thermal analysis for solidification of PCM including nanoparticles within a container. *Case Stud Therm Engineer* 2022;33:101920. [CrossRef]
- [54] Zhao C, Tao Y, Yu Y. Thermal conductivity enhancement of phase change material with charged nanoparticle: A molecular dynamics simulation. *Energy* 2022;242:123033. [CrossRef]
- [55] Wu Y, Rong J, Wang D, Zhao X, Meng L, Arıcı M, et al. Synergistic enhancement of heat transfer and thermal storage characteristics of shell and tube heat exchanger with hybrid nanoparticles for solar energy utilization. *J Clean Prod* 2023;387:135882. [CrossRef]
- [56] Karami R, Kamkari B. Investigation of the effect of inclination angle on the melting enhancement of phase change material in finned latent heat thermal storage units. *Appl Therm Engineer* 2019;146:45–60. [CrossRef]
- [57] Martínez A, Carmona M, Cortés C, Arauzo I. Experimentally based testing of the enthalpy-porosity method for the numerical simulation of phase change of paraffin-type PCMs. *J Energy Storage* 2023;69:107876. [CrossRef]
- [58] Seddegh S, Wang X, Henderson AD. A comparative study of thermal behaviour of a horizontal and vertical shell-and-tube energy storage using phase change materials. *Appl Therm Engineer* 2016;93:348–358. [CrossRef]
- [59] Voller VR, Cross M, Markatos N. An enthalpy method for convection/diffusion phase change. *Int J Numer Methods Engineer* 1987;24:271–284. [CrossRef]
- [60] Afsharpanah F, Izadi M, Hamedani FA, Mousavi Ajarostaghi SS, Yaïci W. Solidification of nano-enhanced PCM-porous composites in a cylindrical cold thermal energy storage enclosure. *Case Stud Therm Engineer* 2022;39:102421. [CrossRef]
- [61] Sheikholeslami M. Numerical analysis of solar energy storage within a double pipe utilizing nanoparticles for expedition of melting. *Sol Energy Mater Sol Cells* 2022;245:111856. [CrossRef]
- [62] Li Z, Shahsavari A, Al-Rashed AAA, Talebizadehsardari P. Effect of porous medium and nanoparticles presences in a counter-current triple-tube composite porous/nano-PCM system. *Appl Therm Engineer* 2020;167:114777. [CrossRef]
- [63] Mourad A, Aissa A, Abed AM, Smaïsim GF, Toghraie D, Fazilati MA, et al. The numerical analysis of the melting process in a modified shell-and-tube phase change material heat storage system. *J Energy Storage* 2022;55:105827. [CrossRef]
- [64] Bellos E, Tzivanidis C. Thermal analysis of parabolic trough collector operating with mono and hybrid nanofluids. *Sustain Energy Technol Assess* 2018;26:105–115. [CrossRef]
- [65] Khanafer K, Vafai K. A critical synthesis of thermophysical characteristics of nanofluids. *Int J Heat Mass Transf* 2011;54:4410–4428. [CrossRef]
- [66] Batchelor G. The effect of Brownian motion on the bulk stress in a suspension of spherical particles. *J Fluid Mech* 1977;83:97–117. [CrossRef]
- [67] Amani M, Amani P, Kasaeian A, Mahian O, Wongwises S. Thermal conductivity measurement of spinel-type ferrite MnFe<sub>2</sub>O<sub>4</sub> nanofluids in the presence of a uniform magnetic field. *J Mol Liq* 2017;230:121–128. [CrossRef]
- [68] Elsayed AO. Numerical study on performance enhancement of solid-solid phase change materials by using multi-nanoparticles mixtures. *J Energy Storage* 2015;4:106–112. [CrossRef]
- [69] Arasu AV, Mujumdar AS. Numerical study on melting of paraffin wax with Al<sub>2</sub>O<sub>3</sub> in a square enclosure. *Int Commun Heat Mass Transf* 2012;39:8–16. [CrossRef]
- [70] Alawi OA, Sidik NAC, Xian HW, Kean TH, Kazi SN. Thermal conductivity and viscosity models of metallic oxides nanofluids. *Int J Heat Mass Transf* 2018;116:1314–1325. [CrossRef]
- [71] Vajjha RS, Das DK. Experimental determination of thermal conductivity of three nanofluids and development of new correlations. *Int J Heat Mass Transf* 2009;52:4675–4682. [CrossRef]
- [72] Daood IY. Effects of nano-fluids types, volume fraction of nano-particles, and aspect ratios on natural convection heat transfer in right-angle triangular enclosure. *Engineer Technol J* 2010;28:5365–5388. [CrossRef]
- [73] Brent A, Voller VR, Reid K. Enthalpy-porosity technique for modeling convection-diffusion phase change: application to the melting of a pure metal. *Numer Heat Transf Part A Appl* 1988;13:297–318. [CrossRef]

- [74] Al-Musawi AIA, Taheri A, Farzanehnia A, Sardarabadi M, Passandideh-Fard M. Numerical study of the effects of nanofluids and phase-change materials in photovoltaic thermal (PVT) systems. *J Therm Anal Calorim* 2018;137:623–636. [\[CrossRef\]](#)
- [75] Patankar S. *Numerical Heat Transfer and Fluid Flow*. Washington, DC: Hemisphere; 1980.
- [76] Leonard BP. A stable and accurate convective modelling procedure based on quadratic upstream interpolation. *Comput Methods Appl Mech Engineer* 1979;19:59–98. [\[CrossRef\]](#)
- [77] Sivaiah S, Murali G, Reddy M, Raju RS. Unsteady MHD mixed convection flow past a vertical porous plate in presence of radiation. *Int J Basic Appl Sci* 2012;1:651–666. [\[CrossRef\]](#)
- [78] Murali G, Paul A, Babu N. Numerical study of chemical reaction effects on unsteady MHD fluid flow past an infinite vertical plate embedded in a porous medium with variable suction. *Electron J Math Anal Appl* 2015;3:179–192. [\[CrossRef\]](#)
- [79] Gadipally D, Gundagani M. Analysis of sores and dufour effects on unsteady MHD convective flow past a semi-infinite vertical porous plate via finite difference method. *Int J Appl Phys Math* 2014;4:332–344. [\[CrossRef\]](#)
- [80] Deepa G, Murali G. Effects of viscous dissipation on unsteady MHD free convective flow with thermophoresis past a radiate inclined permeable plate. *Iran J Sci Technol (Sci)* 2014;38:379–388.
- [81] Sari A, Kaygusuz K. Thermal performance of a eutectic mixture of lauric and stearic acids as PCM encapsulated in the annulus of two concentric pipes. *Sol Energy* 2002;72:493–504. [\[CrossRef\]](#)